SAPIENZA
UNIVERSITÀ DI ROMA

FACOLTÀ DI INGEGNERIA DELL'INFORMAZIONE, INFORMATICA E STATISTICA

Corso di Laurea Magistrale in Ingegneria Elettronica

BEAM DYNAMICS STUDIES TO DEVELOP LHC LUMINOSITY MODEL

RELATORE:
Prof. Luigi Palumbo

CORRELATORE:
Dott. Ioannis Papaphilippou

TESI DI LAUREA DI:
Giovanna Campogiani
Matr. N. 1199609

Anno Accademico 2013 - 2014

Alla mia famiglia

Contents

Chapter 1

Introduction

1.1 CERN Accelerators complex

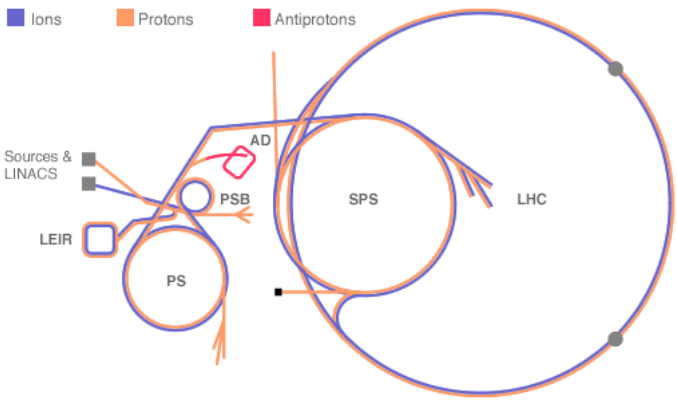

Figura 1.1.1: CERN Accelerators Complex[13]

The accelerator complex at CERN (European Center for Nuclear Research) [4] is a sequence of machines that accelerate charged particles to increasingly higher energies. Each machine boosts the energy of proton beams, before injecting them into the next machine in the sequence. In the Large Hadron Collider (LHC), the last element in this chain, proton beams have been accelerated up to the record energy of 4 TeV per beam (until 2013). The beam energy in the first years after the upgrade occurring in the present long shutdown (approximately 2013-2014) is expected to be around 6.5 TeV, close to the nominal design energy of 7 TeV. Most of the other accelerators in the chain have associated experimental halls where beams are used for experiments at lower energies.

The LHC consists of a 27-kilometers ring of superconducting magnets with a number of accelerating structures to accelerate the particles along the way. Inside the accelerator, two high-energy particle beams travel at close to the speed of light before they are made to collide. The beams travel in opposite directions in separate beam

Machine	Injection Energy [GeV]	Extraction Energy [GeV]
LINAC2	0	0.05
PSB	0.05	1.4
PS	1.4	25
SPS	25	450
LHC	450	7000

Table 1.1.1: Injection and extraction energies of the different machines of the CERN Accelerator complex

pipes – two tubes kept at ultrahigh vacuum ($< 10^{-7}$Pa). They are guided around the accelerator ring by a high magnetic field (8.4 T at nominal design) maintained by superconducting magnets, that form a so called "strong-focusing" periodic lattice.

The electromagnets are built from coils of special electric cable that operates in a superconducting state, efficiently conducting electricity without resistance or loss of energy. This requires the magnets to be brought to the temperture of -271.3°C. For this reason, much of the accelerator is connected to a distribution system of liquid helium, which cools the magnets, as well as to other supply services. Thousands of magnets of different varieties and sizes are used to direct the beams around the accelerator. These include 1232 dipole magnets, each 15 metres long, which bend the beams and 392 quadrupole magnets, each 5–7 metres long, which focus the beams. Just prior to collision, superconducting quadrupoles are used to "squeeze" the particles closer together to increase the chances of collisions.

All the controls for the accelerator, its services and technical infrastructure are housed under one roof at the CERN Control Centre. From here, the beams inside the LHC are made to collide at four locations around the accelerator ring, corresponding to the positions of four particle detectors – ATLAS (IP1), CMS(IP5), ALICE(IP2) and LHCb(IP8). The following table summarizes some of the key parameters of the Large Hadron Collider nominal design parameters.

Quantity	number
Circumference	26 659 m
Dipole operating temperature	1.9 K (-271.3°C)
Number of magnets	9593
Number of main dipoles	1232
Number of main quadrupoles	392
Number of RF cavities	8 per beam
Nominal energy, protons	7 TeV
Nominal energy, ions	2.76 TeV/u (*)
Peak magnetic dipole field	8.33 T
Min. distance between bunches	~7 m
Design luminosity	10^{34} cm^{-2} s^{-1}
No. of bunches per proton beam	2808
No. of protons per bunch (at start)	1.1 x 10^{11}
Number of turns per second	11 245
Number of collisions per second	600 million

(*) Energy per nucleon

Table 1.1.2: Nominal design LHC parameters[4]

1.2 Goal of the thesis

The thesis project aims at studying the different physical processes that are impacting luminosity, one of the key figures of merit of a collider operation. In particular the project focuses on extracting the most relevant parameters for the high-energy part of the model, which is mostly dominated by the beam-beam effect. LHC luminosity is degraded by parasitic collisions that reduce the beam lifetime and the particles stability in the collider. This instability is due to the non-linear effects of one beam electromagnetic field on another in the interaction region. Such parasitic encounters can be as many as 16 per interaction region, piling up to around 180 000 per second. Our goal is to study the evolution of charge density distribution in the beam, by tracking particles through a symplectic integrator that includes the beam-beam effect. In particular we want to obtain data on the halo particles, which are more sensible to instability, to better characterise the beam lifetime and monitor the luminosity evolution.

We will start by presenting some key beam dynamics concepts in chapter 1, with a particular emphasis on the Hamiltonian formalism of the dynamics, which is at the core of the simulation tools used to understand the physical phenomena.

Chapter 2 will present the key elements of collider operations, with a focus on presenting existing luminosity models.

Chapter 3 analyses the details of the beam-beam interaction phenomena, that is the dominant degenerative effect for luminosity and beam lifetime at high energies.

Chapter 4 presents SixTrack, the symplectic integrator developed at CERN to perform beam-beam particle-tracking studies and predict the beam behaviour through evaluation of the particle trajectory along the lattice optics.

Chapter 5 presents the particle tracking methodology and partial results.

Finally, we will present our preliminary conclusions and the steps to further studies.

Chapter 2

Beam dynamics concepts

Particle physics research starting point can be considered Rutherford experiment, that discovered the existence of the atomic nucleus by scattering of helium ions off gold foils. Since then, particle accelerators technologies development has taken off, involving many different branches of science and influencing them. Nowadays, particle accelerators are consolidated tools for both scientific and industrial applications.

In this chapter we will illustrate some basic concepts needed to understand the dynamics of the machines. We will focus in particular on studying the evolution of the system with respect to the plane orthogonal to the one where the accelerator circumference lies. This is called the transverse beam dynamics.

2.1 Charged particle accelerators basics

Relativistic electromagnetism is the fundamental phenomenon on which all particle accelerators technologies are based. Any electrically charged particle with charge q, moving with velocity $\vec{v}$ in an electromagnetic field, interacts with the latter through the Lorentz' force

$$\vec{F} = q(\vec{E} + \vec{v} \times \vec{B}) \tag{2.1.1}$$

where $\vec{E}$ and $\vec{B}$ stand respectively for the electric and the magnetic component of the field. This formula shows that the component of the force generated by the electric field supplies energy to the particle, while the magnetic-generated component of the force can only steer the particle, as it is perpendicular to both $\vec{B}$ and $\vec{v}$.

An accelerator thus uses electromagnetic. fields to guide bunches of charged particles, which are called beams, in vacuum chambers, for acceleration and manipulation.

Any charged particle can be accelerated, with a tailor designed machine to match its intrinsic physical characteristics. The beams are most commonly made of bunches of electrons or protons; nevertheless experiments exist that accelerate positrons, antiprotons or ions. Particles are easily brought to speeds close to the limit one, the speed of light. Special relativity is thus a key ingredient to understand the behaviour of the beams.

The relativistic momentum vector is $\vec{p} = \gamma m_0 \vec{v}$ and describes the dynamic state, wherem_0 represents the rest mass, $\gamma = \frac{1}{\sqrt{1-\beta^2}}$ is the relativistic factor and $\beta = \frac{v}{c}$.

At relativistic velocities, an electric field E and a magnetic field B have the same effect for $E = cB$. A magnetic field of 1 T would then be the equivalent of an electric field of $3 \cdot 10^8 \frac{V}{m}$. Producing such an electric field is far beyond technical limits for current magnet designs, as a result we always use magnetic fields to steer the beams. The physical fundamentals of beam steering and focusing are called *beam optics*, and the study of the properties of the beam influenced by the optics is called *transverse dynamics*. We will study the beam dynamics in what is called the *single particle dynamics* regime, meaning that the collective effects of the particles ensemble in a beam bunch are neglected in our analysis.

Accelerators types Accelerators machine complexes are classified depending on the characteristics of the electromagnetic. fields used for acceleration, and on topology, as table (2.1.1) summarises (altough it does not comprise all the possible machine types).

Accelerators name	Field type		Topology
	E	B	
Electrostatic	Fixed	Fixed	Linear
Betatron	Fixed	Ramping	Circular
Cyclotron	Ramping	Fixed	Circular
LINAC	Pulsed (RF)	Fixed	Linear
Synchrotron	Pulsed (RF)	Ramping synchronously	Circular

Tabella 2.1.1: Summary of charged particles accelerators classification (non exhaustive)

2.2 Lagrangian and Hamiltonian formalism

The Newtonian equations of motion have the disadvantage that they differ in their form markedly when the coordinate system is changed. To circumvent the problem, in classical mechanics one introduces the *generalized coordinates* q_i and the associated velocities $\dot{q}_i$; one defines a function $L = (q_i, q_i, t)$, the Lagrange function, from which the equations of motion can be generated in a form that is independent of the coordinate system. The relativistic Lagrangian of a single particle in an electromagnetic field is

$$L = -\frac{mc^2}{\gamma} - e\phi + e\vec{v} \cdot \vec{A} \tag{2.2.1}$$

where ϕ is the electric scalar potential and $\vec{A}$ is the magnetic vector potential (see Appendix (A) for the Lagrangian derivation). This function is not unique, as it is defined up to an arbitrary costant. Through the Hamilton's principle of stationary action

$$\delta I = \int_1^2 \dot{L}(q_i, \dot{q}_i, t)\, dt = 0 \tag{2.2.2}$$

and the introduction of the canonical or conjugate momentum

$$p_i = \frac{\partial L}{\partial \dot{q}_i} \tag{2.2.3}$$

one obtaines the following Euler-Lagrange equations

$$\sum_{i=1}^{n} \frac{\partial L}{\partial q_i} - \frac{d}{dt}\frac{\partial L}{\partial \dot{q}_i} = 0 \tag{2.2.4}$$

This system of equations enables to "automatically" obtain Newton's equation in any reference frame, by simply plugging the system's Lagrangian in (2.2.4).

Euler-Lagrange equations are second-order differential equations, and hence, the motion of the particle is completely specified if the initial values for the generalised coordinates q_i and velocities $\dot{q}_i$ are known, thus solving the Cauchy problem for the system. For many applications, in particular for numerical techniques of calculating the particle motion, it is more convenient to replace the second-order differential equations with a set of twice the number of first-order differential equations. This is done in the Hamiltonian formulation of classical mechanics, where the general coordinates and velocities $(q_i, \dot{q}_i, t)$ are replaced by (q_i, p_i, t), also known as canonical coordinate and momenta. The change in variables from one set to another is possible with the introduction of the Hamiltonian $H(q_i, p_i, t)$, defined as

$$H(q_i, p_i, t) = \sum_i \dot{q}_i p_i - L(q_i, \dot{q}_i, t)$$

that can be demostrated to be equivalent to the energy of a system. The equations of motion are then found solving the following Hamilton's canonical equations

$$\begin{cases} q_i = \frac{\partial H}{\partial p_i} \\ \dot{p}_i = -\frac{\partial H}{\partial q_i} \\ \dot{H} = -\frac{\partial L}{\partial t} \end{cases} \tag{2.2.5}$$

which constitute a set of $2n$ first-order equations replacing the n Lagrange equations.

The relativistic Hamiltonian of a particle in an electromagnetic field is

$$H = c\left[m^2c^2 + (\vec{p} - e\vec{A})^2\right]^{1/2} + e\phi \tag{2.2.6}$$

where $\vec{p}$ represents the momentum vector, $\vec{A}$ is the magnetic vector potential, ϕ is the electric potential and e is the fundamental particle charge.

In principle, the first step in solving a particular problem of charged particle motion in this canonical formulation is to set up the Lagrangian, from which the Hamiltonian is constructed and then to substitute such function in Hamilton's equations.

Neglecting acceleration, as the longitudinal motion of a particle in an accelerator (synchrotron motion) is much slower than the transverse oscillation, we can neglect the electric potential term $q\phi$.

The Hamiltonian represents the energy of a system; if the system is a conservative one, the Hamiltonian is time-independent and it is an *integral of motion*. Any

variable from which the Hamiltonian is independent is called *cyclic variable*. To study Hamiltonian systems, it is crucial to identify the integrals of motion. To do so, it is convenient to define the Poisson brackets between two functions of a set of canonical variables:

$$[f,g] = \sum_{i=1}^{n} \left(\frac{\partial f}{\partial p_i}\frac{\partial g}{\partial q_i} - \frac{\partial g}{\partial p_i}\frac{\partial f}{\partial q_i} \right) \tag{2.2.7}$$

If a quantity is explicitly time-independent and its Poisson bracket with the Hamiltonian is zero, then it is an integral of motion.

The set of generalised coordinates and conjugate momentas form the *phase space*. Studying the shape of the lines for $H(q_i, p_i) = constant$ one can draw the so called *phase space profiles*, that provide a quick tool for understanding whether the motion of a system is bound or not.

2.2.1 Canonical transformations

If we want to go from a set (q,p) to another set (Q,P) of conjugate momenta, we need to be careful. A transformation of coordinates of this kind will not, in general, lead to phase space coordinates that obey Hamilton's equations (2.2.5), thus not preservig phase space volume [9]. Finding a transformation that ensures the existence and preservation of Hamiltonian equations in the new conjugate momenta set can make the system easier to study without changing its properties. Such a transformation is said to be canonical (or symplectic), and it has the following properties:

$$\begin{cases} \dot{q} = \frac{\partial H(q,p)}{\partial p} & with\ q = (q_1, \dots, q_n) \\ \dot{p} = -\frac{\partial H(q,p)}{\partial q} & with\ p = (p_1, \dots, p) \end{cases} \Longrightarrow \begin{cases} \dot{Q} = \frac{\partial K(Q,P)}{\partial Q} & \text{with } Q = (Q_1, \dots, Q_n) \\ \dot{P} = -\frac{\partial K(Q,P)}{\partial P} & \text{with } P = (P_1, \dots, P_n) \end{cases}$$
$$\cup$$
$$K(Q,P,t) \mid \int [P\dot{Q} - K(Q,P,t)]dt = 0 \tag{2.2.8}$$

As canonical transformations must preserve phase space volume, the following identity must hold:

$$\int \prod_{i}^{n} dp_i dq_i = \int \prod_{i}^{n} dP_i dQ_i \tag{2.2.9}$$

The i-th infinitesimal volume element in the old coordinates can be expressed in the new ones through the Jacobian, as

$$\prod_{i}^{n} dp_i dq_i = \frac{\partial(P_1, \dots, P_n; Q_1, \dots, Q_n)}{\partial(p_1, \dots, p_n; q_1, \dots, q_n)} \prod_{i}^{n} dP_i dQ_i \tag{2.2.10}$$

Putting together equations (2.2.9)and (2.2.10), it follows that the Jacobian of a canonical transformation must always be unitary.

Let's make the hypothesis that we can construct K through an auxiliary function, called the *generating function*. The statements above imply that this function F can be any function of the new and/or old conjugate momenta, and of time. We can then express a generic new Hamiltonian as

$$K(Q,P,t) = H(q(Q,P,t),p(Q,P,t)) + \frac{\partial F_i(q,Q,p,P,t)}{\partial t} \tag{2.2.11}$$

where F defines a canonical transformation from (q,p) to (Q,P).

2.2.2 Frenet-Serret reference frame

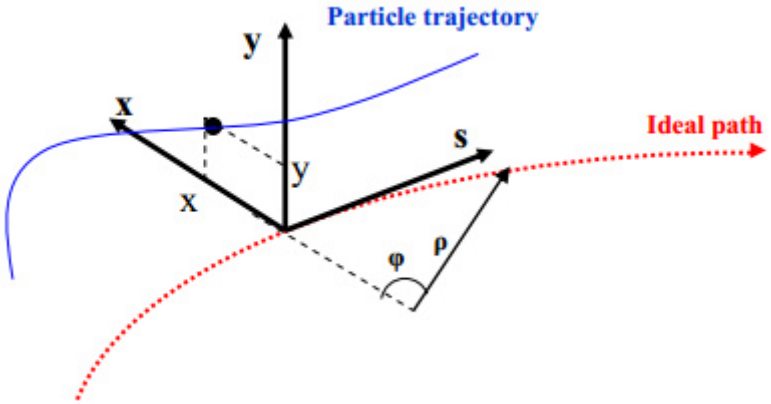

Figura 2.2.1: Reference orbit in the Frenet-Serret reference frame

High energy colliders as the LHC, are usually circular machines, as this enables to use the RF accelerating power for more than one turn. For such geometries, it comes natural to study the beam dynamics through a curviliner coordinate system, rather than the usual cartesian one. As shown in Figure 2.2.1 ,we can define a new reference frame to describe the path of the particles, in which s will describe the longitudinal position of it along the reference orbit. The x and y axis move jointly along the orbit, and define the osculating transverse plane of motion, in terms of deviation from the reference orbit as well. The trajectory has a local radius of curvature ρ. The trajectory of the reference particle r_0 is the one that has null transverse displacement for any value of s. Any particle trajectory around the reference orbit can be expressed as:

$$\vec{r} = \vec{r_0} + x\hat{x}(s) + y\hat{y}(s) \tag{2.2.12}$$

where $\hat{x}$ and $\hat{y}$ are the unit vectors in the transverse plane[19]. We want the new coordinate set to be symplectic, so we look for the canonical transformation

$$\begin{gathered}(q,p,t) \mapsto (Q,P,t) \\ (x,y,z,p_x,p_y,p_z,t) \mapsto (X,Y,s,P_x,P_y,P_s,t)\end{gathered} \tag{2.2.13}$$

In the hypotesis of planar motion, the generating function and the new conjugate momenta are

$$\begin{gathered}F_3 = -\vec{p}\cdot\vec{r} \\ \vec{P} = (P_x,P_y,P_s) = \vec{p}\cdot(\hat{x(s)},\hat{y(s)},(1+\tfrac{x}{\rho})\hat{t})\end{gathered} \tag{2.2.14}$$

yielding the following new Hamiltonian

$$H_{fs}(X,Y,s,P_x,P_y,P_s,t) = c\left[m^2c^2 + (P_x - \frac{e}{c}A_x)^2 + (P_y - \frac{e}{c}A_y)^2 + \frac{(P_s - \frac{e}{c}A_s)^2}{(1+\frac{x}{\rho})^2}\right]^{1/2} \tag{2.2.15}$$

2.2.3 Space as independent variable

As the particle is revolving in a circular periodic orbit, we can take s as the independent variable instead of t. Noticing that the Hamiltonian can be considered as the conjugate momentum of time, we operate the following transformation [29]

$$(x, y, s, p_x, p_y, p_s, t) \mapsto (X, Y, t, P_x, P_y, -H, s) \tag{2.2.16}$$

yielding

$$H_s(X, Y, t, P_x, P_y, -H, s) = -\frac{e}{c}A_s - (1+\frac{x}{\rho})\left[(\frac{H}{c^2} - m^2c^2) + (P_x - \frac{e}{c}A_x)^2 + (P_y - \frac{e}{c}A_y)^2\right]^{1/2} \tag{2.2.17}$$

Finally, we notice that

$$(\frac{H}{c^2} - m^2c^2) = (\frac{E}{c^2} - m^2c^2) = P^2 \tag{2.2.18}$$

2.2.4 Momentum rescaling

In the paraxial hypotesis, $P \gg p_x, p_y$ so we make another canonical transformation

$$(x, y, t, p_x, p_x, p_t, s) \mapsto (X, Y, -ct, \frac{P_x}{P}, \frac{P_y}{P}, -\frac{P_t}{P_0 c}, s) \equiv (\bar{x}, \bar{y}, \bar{t}, \bar{p_x}, \bar{p}_y, \bar{p}_t, s) \tag{2.2.19}$$

where $P_0$is the relativistic momentum of the reference particle and $\bar{p}$ is the angular divergence. This transformation yields the new Hamiltonian

$$H_{parax}(\bar{x}, \bar{y}, \bar{t}, \bar{p_x}, \bar{p}_y, \bar{p}_t, s) = \frac{H_s}{P_0} = -\frac{e}{c}\bar{A}_s - (1+\frac{\bar{x}}{\rho})\left[(\bar{p}_t^2 - \frac{m^2c^2}{P_0}) + (\bar{p}_x - \frac{e}{c}\bar{A}_x)^2 + (\bar{p}_y - \frac{e}{c}\bar{A}_y)^2\right]^{1/2} \tag{2.2.20}$$

where $\bar{A} = \frac{A}{cP_0}$ and $\frac{m^2c^2}{P_0} = \frac{1}{\beta_0^2\gamma_0^2}$, where β_0, γ_0 are the relativistic factors.

2.2.5 Further approximations for large high energy rings

Instead of expressing the longitudinal coordinates in absolute terms, we want to measure the longitudinal position of a particle in tems of distance from the reference particle. We recur once more to a canonial transformation

$$(\bar{x}, \bar{y}, \bar{t}, \bar{p_x}, \bar{p}_y, \bar{p}_t, s) \mapsto (\bar{x}, \bar{y}, \bar{t} + \frac{s - s_0}{\beta_0}, \bar{p_x}, \bar{p}_y, \bar{p}_t - \frac{1}{\beta_0}, s) \equiv (\hat{x}, \hat{y}, \hat{t}, \hat{p}_x, \hat{p}_y, \hat{p}_t) \tag{2.2.21}$$

where $\hat{t}$ stands for the distance from the reference particle, and $\hat{p}$ stands for the relative momentum difference with the reference particle, as shown here:

$$\begin{aligned} \hat{t} = \bar{t} + \tfrac{s-s_0}{\beta_0} = -ct + \tfrac{s-s_0}{v_0}c = c(\Delta t - t) = l \\ \hat{p} = \bar{p}_t - \bar{p}_{t_0} = \tfrac{P-P_0}{P_0} = \delta \end{aligned} \tag{2.2.22}$$

Moreover, in the ultrarelativistic regime, $\beta \to 1 \Rightarrow \frac{1}{\beta_0^2\gamma^2} \to 0$. We ignore the end fields of our lattice elements and we assume that the magnetic field is only transverse,

so that $A_x = A_y = 0$ (good approximation in big accelerators). Including all these considerations, the Hamiltonian becomes

$$H_{ultrarel-refpart}(\hat{x}, \hat{y}, l, \hat{p}_x, \hat{p}_y, \delta) = (1+\delta) - e\hat{A}_s - (1+\frac{\hat{x}}{\rho})\left[(1+\delta)^2 - \hat{p}_x^2 - \hat{p}_y^2\right]^{1/2} \tag{2.2.23}$$

As we are considering high energy particles moving at relativistic velocity in the s direction, the momentum components in the transverse plane are small compared to the total momentum. As $\frac{\hat{p}_x^2+\hat{p}_y^2}{(1+\delta)^2} \ll 1$ we can expand the square root term of (2.2.23) in Taylor series. Moreover, we assume that the radial deviation from the reference orbit is negligible in comparison to the radial curvature ($\frac{\hat{x}}{\rho} \ll 1$), which is a valid approximation for big rings.

In conclusion, the simplified Hamiltonian becomes

$$\hat{H}(\hat{x}, \hat{y}, l, \hat{p}_x, \hat{p}_y, \delta) = -e\hat{A}_s - \frac{\hat{x}}{\rho}(1+\delta) + \frac{\hat{p}_x^2 + \hat{p}_y^2}{2(1+\delta)} \tag{2.2.24}$$

2.3 Multipoles expansion

We now want to find a suitable expression for the magnetic potential in the Frenet-Serret reference frame (x,y,s,t). From the above mentioned assumption of perfect 2D transverse magnetic field, we can thus consider $A_x = A_y = 0$. The differential operator in accelerator coordinates gets scaled as [19]

$$\begin{gathered}\nabla = \frac{1}{h_s}\left[\frac{\partial(h_s A_x)}{\partial x} + \frac{\partial(h_s A_y)}{\partial y} + \frac{\partial A_s}{\partial s}\right] \\ h_s = 1 + \frac{x}{\rho}\end{gathered} \tag{2.3.1}$$

and so

$$\begin{gathered}\vec{B} = B_x(x,y)\hat{x} + B_y(x,y)\hat{y} \\ B_x = (\nabla \times A_s\hat{s})_x = -\frac{1}{h_s}\frac{\partial A_s}{\partial y} \\ B_y = (\nabla \times A_s\hat{s})_y = \frac{1}{h_s}\frac{\partial A_s}{\partial yx}\end{gathered} \tag{2.3.2}$$

Plugging the equations above into Maxwell's equation for a purely magnetic field

$$\nabla \times \vec{B} = 0 \tag{2.3.3}$$

we obtain

$$\frac{\partial}{\partial y}\frac{1}{h_s}\frac{\partial A_s}{\partial y} + \frac{\partial}{\partial x}\frac{1}{h_s}\frac{\partial A_s}{\partial x} = 0 \tag{2.3.4}$$

In a rectangular coordinate system with $h_s = 1$, equation (2.3.4) yields

$$\nabla_\perp^2 A_s = 0 \tag{2.3.5}$$

that can be solved by means of a complex power series as

$$A_s(x,y) = B_0 Re\left\{\sum_{n=0}^{\infty}\frac{b_n + ja_n}{n+1}(x+jy)^{n+1}\right\} \tag{2.3.6}$$

where the costant B_0 is usually chosen as the main dipol strength (i.e. $B_0 = \frac{1}{\rho}\frac{pc}{e}$), such that $b_0 = 1$. From the power series expression of the potential we can now

easily extract a general expression for the effective multipole field on the particles beam, by solving (2.3.2) for (2.3.6), yielding

$$\begin{gathered} B_y + jB_x = B_0 \sum_{n=0}^{\infty} (b_n + ja_n)(x+jy)^n \\ \frac{1}{[B\rho]}(B_y + jB_x) = \mp\frac{1}{\rho} \sum_{n=0}^{\infty} (b_n + ja_n)(x+jy)^n \\ b_n = \frac{1}{B_0 n!} \frac{\partial^n B_y}{\partial x^n}\bigg|_{x=y=0}, \quad a_n = \frac{1}{B_0 n!} \frac{\partial^n B_x}{\partial x^n}\bigg|_{x=y=0} \end{gathered} \tag{2.3.7}$$

The coefficients b_n, a_n are called $(2n+1)th$ multipole coefficients. There is an additional distinction then between the b_n ones, which are called *normal multipole* components, when the magnet gap lies on the horizontal plane; a_n coefficients are instead called *skew multipole* components. The complex 2D magnetic field representation $B_y + jB_x$ is called the Beth representation.

Normal dipole $(n = 1)$: $b_1 \cdot B_{main} = B_{vert}$ (horizontally bending)	
$B_\varphi(r,\varphi) = B_{vert} \cdot \cos\varphi$	$B_r(r,\varphi) = B_{vert} \cdot \sin\varphi$
$B_x(x,y) = 0$	$B_y(x,y) = B_{vert}$
Skew dipole $(n = 1)$: $a_1 \cdot B_{main} = B_{hor}$ (vertically bending)	
$B_\varphi(r,\varphi) = B_{hor} \cdot \sin\varphi$	$B_r(r,\varphi) = -B_{hor} \cdot \cos\varphi$
$B_x(x,y) = -B_{hor}$	$B_y(x,y) = 0$
Normal quadrupole $(n = 2)$: $b_2 \cdot B_{main} = -g \cdot r_0$ (where g is the gradient)	
$B_\varphi(r,\varphi) = -gr\cos 2\varphi$	$B_r(r,\varphi) = -gr\sin 2\varphi$
$B_x(x,y) = -gy$	$B_y(x,y) = -gx$
Skew quadrupole $(n = 2)$: $a_2 \cdot B_{main} = -g \cdot r_0$ (quadrupole rotated by 45°)	
$B_\varphi(r,\varphi) = -gr\sin 2\varphi$	$B_r(r,\varphi) = gr\cos 2\varphi$
$B_x(x,y) = gx$	$B_y(x,y) = -gy$
Normal sextupole $(n = 3)$: $b_3 \cdot B_{main} = \frac{1}{2}g' \cdot r_0^2$	
$B_\varphi(r,\varphi) = \frac{1}{2}g'r^2\cos 3\varphi$	$B_r(r,\varphi) = \frac{1}{2}g'r^2\sin 3\varphi$
$B_x(x,y) = g'xy$	$B_y(x,y) = \frac{1}{2}g'(x^2 - y^2)$

Figura 2.3.1: Summary of the multipole coefficients for dipole, quadrupole and sextupole fields in Beth representation [10]

2.3.1 Linear optics Hamiltonian

We complete the Hamiltonian adding to it the explicit expression of the magnetic potential for linear fields. Using the multipole expansion (2.3.6) of the magnetic

potential and (2.3.2) we obtain

$$\begin{cases} B_x = b_1(s)y = -\frac{1}{1+\frac{x}{\rho}}\frac{\partial A_s}{\partial y} \\ B_y = -b_0(s) + b_1(s)x = \frac{1}{1+\frac{x}{\rho}}\frac{\partial A_s}{\partial x} \end{cases} \tag{2.3.8}$$

Integrating the aforementioned expressions, we obtain

$$A_s(x,y,s) = \frac{P_0 c}{e}\left[-\frac{x}{\rho} - (\frac{1}{\rho^2}+k)\frac{x^2}{2} + k\frac{y^2}{2}\right] = P_0 c\hat{A}_s(x,y,s) \tag{2.3.9}$$

Plugging (2.3.9) into (2.2.24) we obtain

$$H(\hat{x},\hat{y},l,\hat{p}_x,\hat{p}_y,\delta) = \frac{\hat{p}_x^2+\hat{p}_y^2}{2(1+\delta)} - \frac{x\delta}{\rho} + \frac{x^2}{2\rho^2} + \frac{k}{2}(x^2-y^2) \tag{2.3.10}$$

Now we can simply derive the equations of motion from plugging the Hamiltonian into Hamilton's equations, as follows

$$\begin{cases} \frac{\partial x}{\partial s} = \frac{\partial H}{\partial p_x} = \frac{2p_x}{2(1+\delta)}; & \frac{\partial p_x}{\partial s} = -\frac{\partial H}{\partial x} = \frac{\delta}{\rho} - \frac{2x}{2\rho^2} - kx \\ \frac{\partial y}{\partial s} = \frac{\partial H}{\partial p_y} = \frac{p_y}{(1+\delta)}; & \frac{\partial p_y}{\partial s} = -\frac{\partial H}{\partial y} = -ky \end{cases} \tag{2.3.11}$$

Putting them together line by line, we get a set of two second order differential equations, called Hill's or betatron equations

$$\begin{cases} x'' - (k - \frac{1}{\rho^2})x = \frac{\delta}{\rho} \\ y'' + ky = 0 \end{cases} \tag{2.3.12}$$

that can be rewritten as

$$\begin{cases} x'' + K_x(s)x = \frac{\delta}{\rho} \\ y'' + K_y(s)y = 0 \end{cases} \tag{2.3.13}$$

In an actual accelerator the magnetic fields change with time, and there are longitudinal electric fields to accelerate the particles. However, the acceleration process is slow, so it can be considered adiabatic for our purposes.

2.4 Dispersion

The horizontal term of our equation of motion has a non-zero term on the right side, so it is an inhomogeneous differential equation. Its solution is given by a linear superposition of the particular solution and the solution of the homogeneous equation, so we can write

$$x(s) = x_H + x_P = x_H + \delta D(s) \tag{2.4.1}$$

where

$$D(s) = \frac{x_P(s)}{\delta} \tag{2.4.2}$$

is called the *dispersion function*, or the off-momentum closed orbit, and relates the spread in momentum to the position displacement from the ideal orbit. Plugging (2.4.1) into (2.3.13) we obtain

$$x''_H + K_x(s)x_H + \delta(D'' + K_x(s)D) = \frac{\delta}{\rho} \Longleftrightarrow \begin{cases} x''_H + K_x(s)x_H = 0 \\ D'' + K_x(s)D = \frac{1}{\rho} \end{cases} \tag{2.4.3}$$

The phenomenum of dispersion is intrinsic to the nature of the linear optical elements of an accelerator lattice, whose bending and focusing properties depend on particle's momentum: a more energetic particle will be less bended in a dipole and less focused in a quadrupole, in analogy with chromatic aberration behaviour of light optics lenses. Infact, the term dispersion is mutuated from the symmetrical behaviour of light rays traversing matter, that travel through the material with different velocities depending on the wave number, wave counterpart of momentum. The dependence of focusing on momentum brings in its wake a dependence of the tune on momentum.

Let us analyse mathematically the dependence of quadrupole focusing/defocusing strength from angular momentum, by recalling that, for an horizontally focusing quadrupole

$$k = \frac{e}{p}\frac{\partial B_y}{\partial x} = \frac{e}{p_0(1+\delta)}\frac{\partial B_y}{\partial x} = \frac{k_0}{(1+\delta)} = k_0(1-\delta+O(\delta^2)) \simeq k_0 - k_0\delta \tag{2.4.4}$$

Therefore a particle with a larger energy sees a weaker focusing strength. Conversely for light, the variation of the refraction index with the wavelength can be either positive or negative and the chromatic effect can be corrected to first order by combining lenses of different material.

2.5 Particle trajectory evolution

The general solution of equation (2.4.3) can be written as [10]

$$x(s) = C(s)\, x_0 + S(s)\, x'_0 + D(s)\, \delta \tag{2.5.1}$$

Here x_0, x'_0 are the initial values of the horizontal position and divergence at $s = s_0$, while $C(s)$ and $S(s)$ are two independent solutions of the homogeneous Hill's equation for the reference particle, meaning

$$\begin{aligned} C(s)'' + K(s)C(s) = 0 \\ S(s)'' + K(s)S(s) = 0 \end{aligned} \tag{2.5.2}$$

For the two solutions to be linearly independent, the Wronskian must satisfy the condition

$$W = \begin{vmatrix} C & S \\ C' & S' \end{vmatrix} \neq 0 \tag{2.5.3}$$

As the derivative of the Wronskian vanishes identically as

$$\frac{d}{ds}\left(CS' - SC'\right) = \frac{d}{ds}W = CS'' - SC'' = -K\left(CS - SC\right) = 0 \tag{2.5.4}$$

then the value of W is determined everywhere by the initial conditions at $s = s_0$. We choose

$$C_0 = 1,\ C_0' = 0;\ S_0 = 0,\ S_0' = 1 \tag{2.5.5}$$

The solutions satisfying such initial conditions everywhere are called respectively "Cosinelike" and "Sinelike" principal trajectories, and they result in $W = 1$.

The position and transverse divergence at any point along the ring are related to their initial values by the linear transformation

$$\begin{pmatrix} x \\ x' \end{pmatrix} = \begin{pmatrix} C & S \\ C' & S' \end{pmatrix} \begin{pmatrix} x_0 \\ x_0' \end{pmatrix} + \delta_0 \begin{pmatrix} D \\ D' \end{pmatrix} \tag{2.5.6}$$

that can be rewitten as

$$\begin{pmatrix} x \\ x' \\ \delta \end{pmatrix} = \begin{pmatrix} C & S & D \\ C' & S' & D' \\ 0 & 0 & 1 \end{pmatrix} \begin{pmatrix} x_0 \\ x_0' \\ \delta_0 \end{pmatrix}$$

The dispersion trajectory can be calculated from the principal trajectories as

$$D(s) = S(s) \int_{s_0}^{s} \frac{1}{\rho(t)} C(t)dt - C(s) \int_{s_0}^{s} \frac{1}{\rho(t)} S(t)dt \tag{2.5.7}$$

The solution for the complete "lattice" of magnetic elements is then just the product of the individual matrices in the desired sequence. The matrix formalism moreover justifies the fact that the magnetic elements lattice is also called "the optics", as it is easy to see the analogy with the geometrical optics formalism.

Let us consider a general magnet containing only linear multipoles (i.e. dipole and quadrupole). Assuming the field inside the magnet to be independent of the longitudinal position and to end abruptly at its edges (hard edge model), then the principal trajectories solve Hill's equation

$$z'' + Kz = 0 \ with \begin{cases} K = k \ for \ z = y \\ K = -k + \frac{1}{\rho} \ for \ z = x \end{cases} \tag{2.5.8}$$

So the solution inside the magnet will be

$$\begin{pmatrix} C & S \\ C' & S' \end{pmatrix} = \begin{pmatrix} \cos\phi & \frac{1}{\sqrt{|K|}} \sin\phi \\ -\sqrt{|K|} sin\phi & \cos\phi \end{pmatrix} \quad for\ K > 0\ (focusing) \tag{2.5.9}$$

$$\begin{pmatrix} C & S \\ C' & S' \end{pmatrix} = \begin{pmatrix} \cos\phi & \frac{1}{\sqrt{|K|}} \cos\phi \\ -\sqrt{|K|}\cos\phi & \cos\phi \end{pmatrix} \quad for\ K < 0\ (defocusing) \tag{2.5.10}$$

$$\begin{pmatrix} C & S \\ C' & S' \end{pmatrix} = \begin{pmatrix} 1 & L \\ 0 & 1 \end{pmatrix} \qquad for\ K = 0\ (drift\ space) \tag{2.5.11}$$

where $\phi = L\sqrt{|K|}$ and L is the length of the optical element.

In many practical cases, the distance at which particles get focused by a quadrupole magnet is much larger than the length of the magnet itself. We can then rewrite equation (2.5.9) in the limit of $L \to 0$ as

$$\lim_{L\to 0} \begin{pmatrix} \phi & \frac{1}{\sqrt{|K|}} \sin\phi \\ -\sqrt{|K|}\sin\phi & \cos\phi \end{pmatrix} = \begin{pmatrix} 1 & 0 \\ -|K|\,L & 1 \end{pmatrix} = \begin{pmatrix} 1 & L \\ -\frac{1}{f} & 1 \end{pmatrix} \tag{2.5.12}$$

The true length of the magnet has to be recovered by two drift spaces $l/2$ on either side. This is called the *thin lens approximation* and works accurately for accelerators in the TeV range, where $\frac{1}{\rho^2} \ll |k| \ll \frac{1}{L^2}$.

2.6 Betatron oscillations and Courant-Snyder invariant

In the previous paragraphs we have solved the homogeneous equation of motion in a piecewise manner (with $K(s) = const$ in each piece) and have combined them using matrix algebra. We shall now present a closed form solution of the transverse oscillations for the reference particle, meaning we consider a particle with the design momentum, so that $\delta = 0$. Its evolution in the transverse plane depends on the longitudinal position as follows

$$\begin{aligned} z(s) &= \sqrt{\epsilon\beta(s)}\cos(\psi(s)+\phi) \\ z'(s) &= -\sqrt{\tfrac{\epsilon}{\beta(s)}}[\alpha_z\cos(\psi(s)+\phi)+\sin(\psi(s)+\phi) \end{aligned} \quad with \quad z = x, y \tag{2.6.1}$$

where ϵ is the *emittance* which is equal to the area of the ellipse in the phase space (x,x') (optionally divided by π) and is constant, as Liouville's theorem states; $\beta(s)$ is the *betatron or amplitude function*, a periodic function given by focusing elements of the lattice (i.e. quadrupoles) that represents the envelope of the betatron oscillation, name that indicates the transverse motion of a particle; $\psi(s)$ the *phase advance* and ϕ is the initial phase.

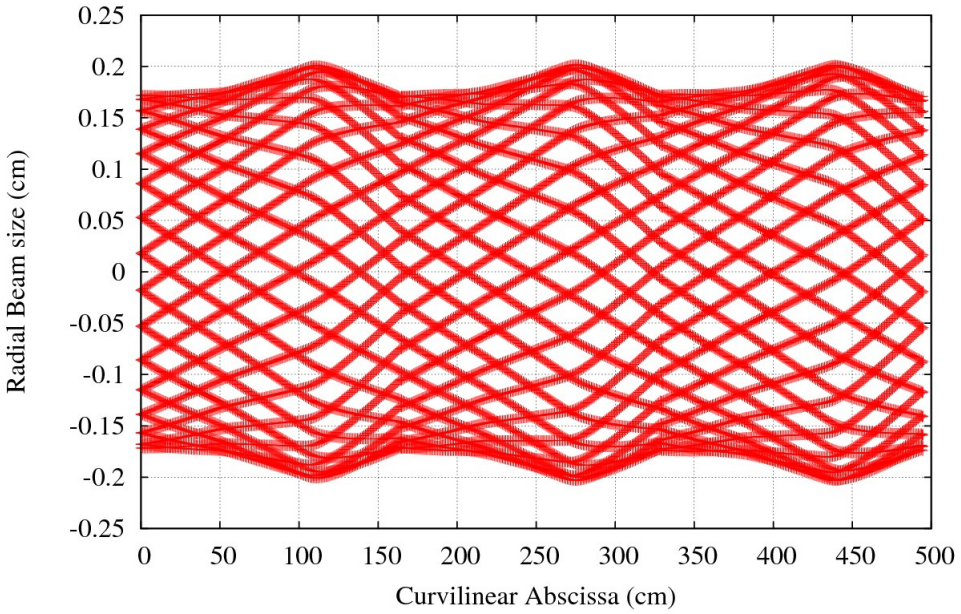

Figura 2.6.1: Within the magnet structure, which has a net focusing effect, the particles perform betatron oscillations with a position-dependent amplitude within the envelope $E(s) = \sqrt{\epsilon\beta(s)}$

The betatron function and the emittance are related through the Courant-Snyder invariant relation, which is basically the ellipse equation in phase space, as follows:

$$\gamma(s)z^2 + 2\alpha(s)zz' + \beta(s)z'^2 = \epsilon \tag{2.6.2}$$

where the quantities $\alpha = -\beta'/2$; β; $\gamma = \frac{1+\alpha}{\beta}$ are called the *Twiss parameters*.

If the Hamiltonian of the system is time-independent, so energy is conserved, then according to Liouville's theorem the particle phase-space flow behaves like an uncompressible fluid, so the volume of the phase space is conserved throughout the time evolution of the system. Each slice in the transverse phase space then also has an invariant area, whose value is exactly the Courant-Snyder invariant. So the orientation and shape of the ellipse change along the trajectory, but not the area.

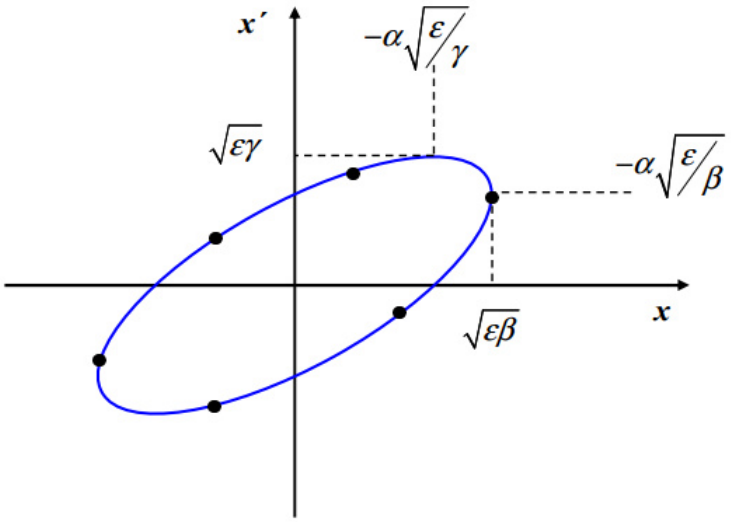

Figura 2.6.2: Courant-Snyder invariant parameters in (x,x') phase space for a single particle [3]

Neglecting mutual interactions and coupling between planes, one defines the emittance for each degree of freedom of the system: horizontal, vertical and longitudinal. There are, however, many particles in a beam, moving with various amplitudes and each corresponding to a different ellipse in the phase space plane. There are different practical definition of beam emittance, for both $z = x, y$:

- The rms emittance of the beam is defined as the area (optionally divided by π) of the ellipse containing 39% of the particles, and if the distribution is a bidimensional Gaussian normal distribution then $\epsilon_{rms\,z} = \frac{\langle z^2(s)\rangle}{\beta(s)} = \frac{\sigma_z^2(s)}{\beta_z(s)}$
- The 95% emittance of the beam is defined as the area (optionally divided by π) of the ellipse containing 95% of the particles, and if the distribution is Gaussian it values $\epsilon_{95\%\,z} = 6\frac{\langle z^2(s)\rangle}{\beta(s)} = 6\frac{\sigma_z(s)}{\beta_z(s)}$

where σ_z is the r.m.s. transverse beam size defined as

$$\sigma_z = \sqrt{\beta_z \epsilon_z} \quad \text{with } z = x,\, y \tag{2.6.3}$$

Analogously we can define an r.m.s. beam divergence as

$$\sigma_{p_z} = \sqrt{\gamma_z \epsilon_z} \text{ with } z = x,\, y \tag{2.6.4}$$

It is useful also to define the *normalised emittance* ϵ_n, that is a relativistic invariant of the beam and is calculated as

$$\epsilon_n = \frac{p_0}{m_0 c}\epsilon = \gamma\beta\epsilon \tag{2.6.5}$$

where $\gamma = \frac{1}{\sqrt{1-\beta^2}}$ and $\beta = \frac{v}{c}$ are the relativistic factors.
When operating an accelerator it is important to ensure that the beam has sufficient room available in the transverse phase space. Even particles undergoing extremely large betatron oscillations can then still circulate stably. The largest phase space ellipse allowed within the vacuum chamber geomatrical radius r, is called the *transverse acceptance* of the accelerator, and is defined as

$$A = \left(\frac{r^2}{\beta}\right)_{min} \tag{2.6.6}$$

where r and β are the values at the narrowest optical position. In order for the beam to circulate with no losses, it is required that $A/\epsilon \gg 1$.

2.7 The tune

Plugging (2.6.1) in the homogenous version of (2.6.1), we obtain the following equation

$$\sqrt{\epsilon\beta}\left\{\left[\psi'' + \frac{\beta'}{\beta}\psi'\right]\cos[\psi(s)+\phi] + \left[-\frac{1}{4}\frac{(\beta')^2}{\beta} + \frac{1}{2}\frac{\beta''}{\beta} - (\psi')^2 + K\right]\sin[\psi(s)+\phi]\right\} = 0 \;\forall\epsilon,\phi \tag{2.7.1}$$

This can be then conveniently rewritten as a system of two equations

$$\begin{cases} \psi'' + \frac{\beta'}{\beta}\psi' = 0 \\ -\frac{1}{4}\frac{(\beta')^2}{\beta} + \frac{1}{2}\frac{\beta''}{\beta} - (\psi')^2 + K = 0 \end{cases} \tag{2.7.2}$$

Let us reorder each differential equation in the form

$$\begin{cases} \psi' = \frac{1}{\beta} \\ \frac{1}{2}\beta'' - \frac{1}{4}\beta'^2 + K\beta - \frac{1}{\beta} = 0 \end{cases} \tag{2.7.3}$$

From here we can directly integrate the first expression and multiply by β both terms of the second equation, yielding

$$\begin{cases} \psi_{tot} = \oint \frac{1}{\beta(s)}ds \\ \frac{1}{2}\beta\beta'' - \frac{1}{4}\beta\beta'^2 + K\beta^2 = 1 \end{cases} \tag{2.7.4}$$

The first equation of the set (2.7.4) is the total phase advance around the accelerator's circumference, for one turn. We can rewrite it as

$$\psi_{tot} = 2\pi\nu = \oint \frac{ds}{\beta(s)} \tag{2.7.5}$$

where ν is called the *tune* and represents the total number of oscillations over one full turn of the machine in a given transverse direction (x or y). From (2.7.5) we immediately obtain

$$\nu = \frac{1}{2\pi} \oint \frac{ds}{\beta(s)} \tag{2.7.6}$$

A quadrupolar field error induces a tune shift Δv that is

$$\Delta\nu = \frac{1}{4\pi} \int_{s_0}^{s_0+l} \Delta k \beta(s) ds \tag{2.7.7}$$

where Δk is the error strength and l is the length of the magnetic element.

2.8 Chromaticity

The parameter quantifying the relationship between tune spread and momentum spread is the chromaticity, defined as

$$\xi(\delta) = \frac{\Delta v}{\delta} \tag{2.8.1}$$

and it can be calculated as

$$\xi(\delta) = \frac{1}{4\pi} \oint K(s)\beta(s) ds \tag{2.8.2}$$

In strong focusing lattices the main contribution to the chromaticity is due to the quadrupoles and to dipole vertical fringe fields.

To correct the chromaticity nonlinear elements sextupole magnets, whose gradient depends quadratically on the betatron amplitude, have to be introduced into the lattice. Sextupoles don't affect the partiles with nominam momentum, while for particles along a dispersive trajectory i.e. $x_D \neq 0$ the sextupole field contributes to an additional quadrupole strenght of

$$k_{sext} = mD\delta \tag{2.8.3}$$

The effective total chromaticity then becomes

$$\xi_{tot}(\delta) = \frac{1}{4\pi} \oint \left[m(s)D(s) + k(s)\right] \beta(s) ds \tag{2.8.4}$$

and in principle it is always possible to choose the number, position and strengths of the sextupoles so that this integral vanishes.

2.9 Normalised coordinates - Floquet's transformation

Let's introduce a new independent variable, a "reduced phase" as

$$\phi = \frac{\psi}{\nu} \tag{2.9.1}$$

so that ϕ is a variable that increases by 2π for each turn, thus behaving like it was a polar angle measured from the center of a circle.

Now we introduce a new dependend variable, namely

$$\begin{gathered} \mathcal{U}(\phi) = \frac{u}{\sqrt{\beta}} = \sqrt{\epsilon}\cos(\nu\phi + \delta) \\ \Downarrow \\ \mathcal{U}' = \frac{d\mathcal{U}}{d\phi} = -\sqrt{\epsilon}\sin(\nu\phi + \delta) = u'\sqrt{\beta} + \frac{u\alpha}{\sqrt{\beta}} \end{gathered} \tag{2.9.2}$$

where δ is the same initial phase advance as before, renamed not to be confused with the new variable. With this change of variable, the free betatron oscillation reduces to simple harmonic motion, with ν oscillations for every phase advance of ϕ by 2π. So we have operated a transformation from

$$(u_x, u_y, s, p_x, p_y, p_s, t) \mapsto (\mathcal{U}_x, \mathcal{U}_y, \phi, \frac{d\mathcal{U}_x}{d\phi}, \frac{d\mathcal{U}_y}{d\phi}, t) \tag{2.9.3}$$

which is called a *Floquet's transformation*, and that transforms the phase space from an ellipse into a circle.

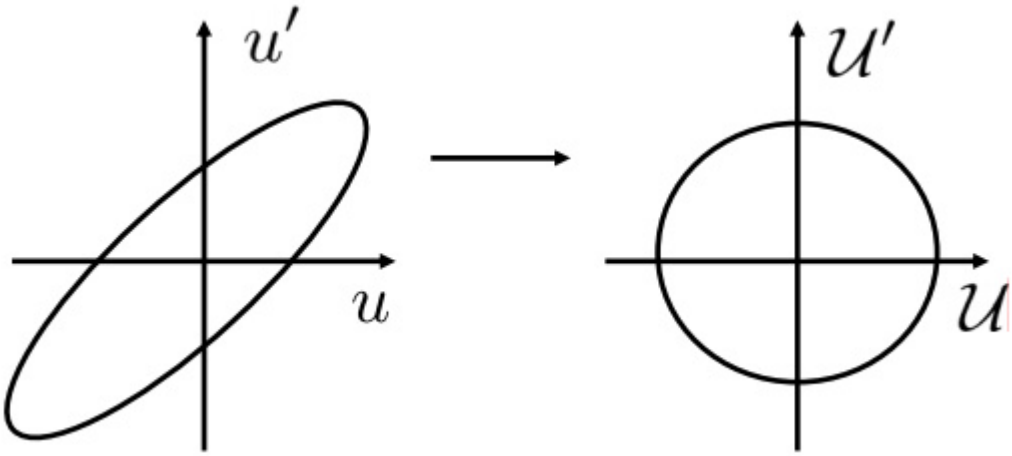

Figura 2.9.1: Phase space mapping through Floquet's transformation

In this reference frame, the equation of motion yield the following differential equation

$$\frac{d^2\mathcal{U}}{d\phi^2} + \nu^2\mathcal{U} = 0 \tag{2.9.4}$$

that enables us to treat the system as a simple harmonic oscillator.

If we consider the equivalent inhomogeneous equation, that is the case when we consider magnet errors and dispersion, in Floquet's coordinate the full collection of mathematical methods for treating driven harmonic resonance become available, and the notion of a resonance between some harmonic amplitude of the driving term and the tune is just the same as in the case of a simple harmonic oscillator.

2.10 Action-angle variables

Canonical transformations enable to simplify the analysis of the motion. A particularly simple way of making the equations of motion integrable, is to consider a transformation that satisfies the following Hamilton-Jacobi equation

$$\mathcal{H}(Q,P,t) = H(q,p,t) + \frac{\partial F}{\partial t} = 0 \tag{2.10.1}$$

In the new coordinates, Hamilton's equations are

$$\begin{cases} \frac{\partial Q}{\partial t} = \frac{\partial \mathcal{H}}{\partial P} = 0 \\ \frac{\partial P}{\partial t} = -\frac{\partial \mathcal{H}}{\partial Q} = 0 \end{cases} \tag{2.10.2}$$

which can be integrated straightforward.
A less strict condition that enables us to quickly simplify the problem is also

$$\mathcal{H} = H + \frac{\partial F}{\partial t} = const. = \lambda P = \mathcal{H}(P) \tag{2.10.3}$$

where P is an integral of motion. This yields the following Hamilton's equations

$$\begin{cases} \frac{\partial Q}{\partial t} = \frac{\partial \mathcal{H}}{\partial P} = \lambda + cost \\ \frac{\partial P}{\partial t} = -\frac{\partial \mathcal{H}}{\partial Q} = 0 \end{cases} \tag{2.10.4}$$

Let's now define the *action integral* J_i is defined by

$$J_i = \oint p_i dq_i \tag{2.10.5}$$

The integration is over a complete cycle of the periodic coordinateq_i. The Hamiltonian becomes

$$\mathcal{H} = \mathcal{H}(J) \mid \begin{cases} \dot{\phi} = \omega(J) \\ \dot{J} = 0 \end{cases} \implies \begin{cases} \phi = \omega(J)t + \phi_0 \\ J = 2\epsilon = cost \end{cases} \tag{2.10.6}$$

For the reference particle in a circular accelerator of high energy, with a big circumference, in the paraxial approximation, the Hamiltonian in action-angle variables is

$$\mathcal{H}_0 = \frac{J_x}{\beta_x(s)} + \frac{J_y}{\beta_y(s)} \tag{2.10.7}$$

2.11 Resonances

Inhomogeneous Hill's equation, after undergoing a Floquet's transformation, becomes

$$\mathcal{U}'' + \nu^2 \mathcal{U} = \nu^2 \beta^{3/2} F(\mathcal{U}_x(\phi_x), \mathcal{U}_y(\phi_y)) \tag{2.11.1}$$

where F is the Lorentz force from perturbing fields, including not only linear magnet imperfections but also non-linear magnetic field errors, wake-fields, space-charge

effects and beam-beam interactions. To find the solution we have to solve a forced harmonic oscillation ODE, whose general form is

$$f''(\phi) + \omega_0^2 f(\phi) = g(\phi) \tag{2.11.2}$$

Moreover, as we are analysing circular accelerators, we have to take into account that the perturbation is periodic. Any periodic function $g(\phi)$ can be expanded in Fourier series as

$$g(\phi) = \sum_{m=-\infty}^{\infty} g_m \exp[im\omega\phi] \tag{2.11.3}$$

The particular solution of the ODE will thus need to have the same form, so we can write the general solution as a combination of the homogeneous unperturbed harmonic oscillator one and the particular one

$$f(\phi) = f_H(\phi) + f_P(\phi) = sin(\omega_0\phi + t) + \sum_{m=-\infty}^{\infty} f_m \exp[im\omega\phi] \tag{2.11.4}$$

Plugging (2.11.4) into (2.11.2) we obtain

$$-m^2\omega^2 f_m + \omega_0^2 f_m = g_m \implies f_m = \frac{g_m}{\omega_0^2 - m\omega^2} \tag{2.11.5}$$

The above equation proves that in such a system exist an infinite number of resonant frequencies, satisfying the relation $\omega_0 = m\omega$.

When the transverse tune satisfies the resonance condition

$$n_x Q_x + n_y Q_y = p \tag{2.11.6}$$

the effect of a perturbation becomes important, the amplitude of the motion may grow rapidly and the particle can be lost. This is why in the circular accelerators we try to have a tune far away from any integer and rational values. In addition if we define the *order of resonance* as

$$N = |n_x| + |n_y| \tag{2.11.7}$$

We see that the destabilizing effects are more important for smaller resonance order, so that it is better to stay away from resonance lines of lower order.

Identification of a resonance inherently consists of picking out the terms from the equations of motion which allow secular growth. For stable operations a pair of values for Q_x and Q_y must be chosen to avoid optical resonances. This pair of values is termed the *working point.* The optical resonances are shown, up to 12th order, for both planes as lines in the diagram in Fig. 2.11.1. Care must be taken to chose a working point that is sufficiently far from these lines.

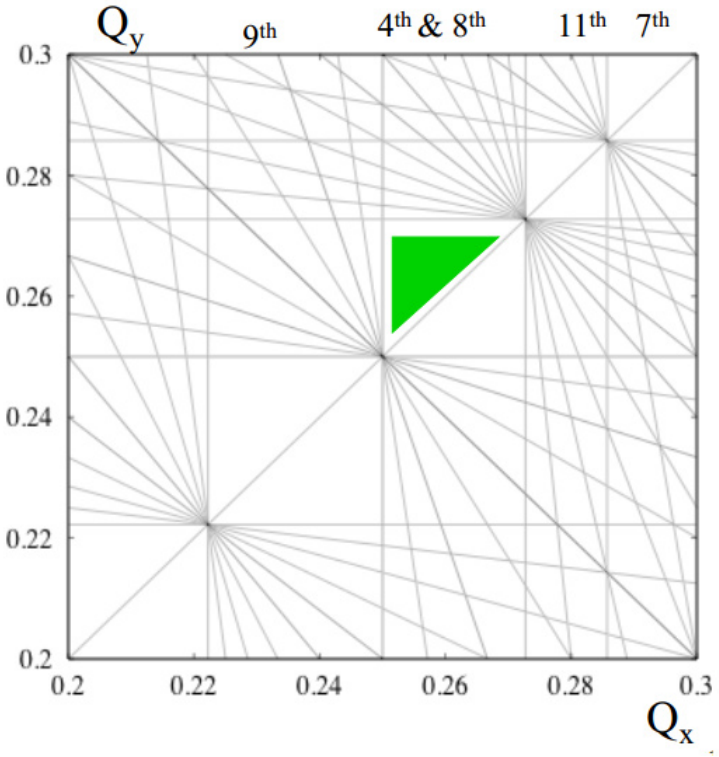

Figura 2.11.1: Tune diagram. The coloured area highlights a part of the tune space free from low order resonance lines, as an example of where to place the working point to have it stable.[28]

2.11.1 Intuitive representation of resonances

We will briefly present what happens in the case in which there is a sextupole in the lattice and the horizontal tunes of the betatron oscillation is equal to one third of an integer.

The kick a particle receives from passing in a sextupole magnet depends on the square of its position and its phase. If the tune is $1/3$, then every three turns correspond to a $2\pi/3$ shift in betatron phase. As shown in the picture below, every three turns the particle returns to the initial position plus an offset, and so its betatron horizontal oscillations, if left uncompensated from this effect, would grow quickly to exceed the beam pipe boundaries, causing particle loss in the beam.

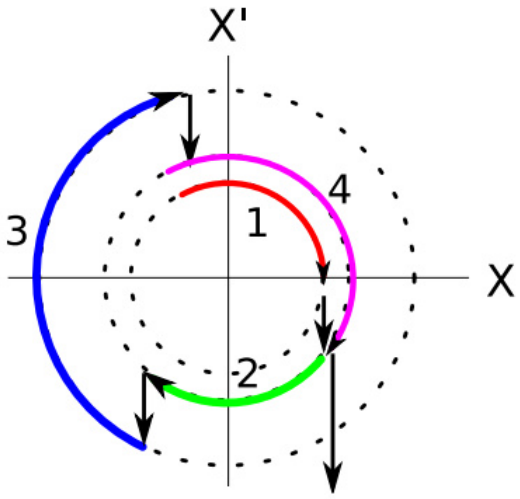

Figura 2.11.2: Normalised phase space of a particle with $Q_x = 1/3$ receiving a sextupolar kick. The plot illustrates how the amplitude grows after three consecutive turns.

Chapter 3

Colliders

Fundamental physics has been extensively using particles accelerators to study the properties of matter that existed in a stable form only moments after the Big Bang. To be able to recreate such particles and states of matter, high energy beam of charged particles are pushed to hit matter and the induced transmutation of energy in mass is studied through detectors. The collision between a beam and a target is thus an elastic collision and beams can be, in first approximation, treated as rigid bodies hitting other rigid bodies.

3.1 Collider performance

The goal of high energy colliders is to produce a high number of events of transmutation of regular matter into unstable and exotic states of itself, to study their properties. For each collision, there is a finite probability of producing a state of interest. Energy is directly related to mass, so the higher the energy, the higher the diversity of states of matter that can be produces. The higher the number of collisions, the higher the probability that from one of them the desired matter state will stem. So, the main parameters that characterize the performance of a collider are:

- available center of mass energy
- number of interactions per second (useful collisions)
- total number of interactions *(beam lifetime)*

3.1.1 Available center of mass energy

There are two possibilities as to what to collide a beam of accelerated particles with:

1. collision with another beam;
2. collision with a fixed target.

The kinematics of a particle with mass m can be expressed by its energy E and momentum $\vec{p}[\frac{eV}{c}]$. These form the components of the invariant energy-momentum 4-vector

$$\vec{P} = (E, \vec{p}) \qquad | \qquad \left\|\vec{P}\right\| = \sqrt{E^2 - p^2} = m_0$$

Given two particles with respective energy-momentum 4-vector $\vec{P_1} = (E_1, p_1)$,$\vec{P_2}$=(E_2,p_2) and masses $m_1 = m_2 = m$, the centre of mass energy resulting from a collision will be, in general:

$$E_{cm} = \sqrt{(E_1 + E_2)^2 - (p_1 + p_2)^2} \tag{3.1.1}$$

A fixed target can be considered as a beam with no velocity, i.e. $\vec{p_2} = 0$. On the other hand, in a collision between two beams the center of mass of the collision point is at rest in the laboratory frame, i.e. $\vec{p_2} = -\vec{p_1}$. The resulting obtainable energies are, thus:

	Momentum	Resulting center of mass Energy	7 TeV proton collision
Fixed target	$p_2 = 0$	$E_{cm} = \sqrt{2m_0^2 + 2m_0E_1}$	$\simeq 115\,GeV$
Beam-beam collision	$\vec{p_2} = -\vec{p_1}$	$E_{cm} = \sqrt{(E_1 + E_2)^2}$	$14\,TeV$

Table 3.1.1: Obtainable energy comparison between fixed target and beam-beam collisions

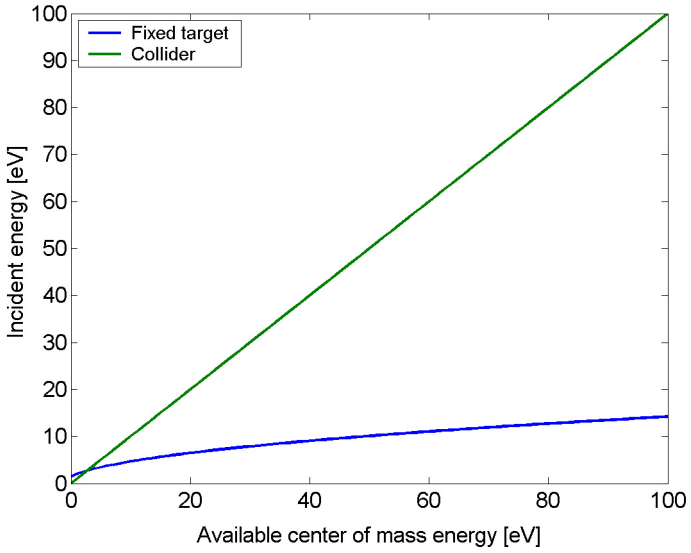

Figure 3.1.1: Center of mass energy growth rate with incident beam energy

Nevertheless, the particle density in a beam is much lower than in a solid or liquid target, therefore one tries to cross the beams many times and maximize the beam intensities (i.e. the number of particle bunches per beam). That's why the choice of a circular collider, with the possibility of passing the same beam several times through the same interaction point, has been a natural choise for high energy physics studies. We will discuss more in details the parameters of colliders' performance in the next section.

3.1.2 Machine operation

When operating a collider we can identify different stages, namely:

- injection phase, which starts with the first bunch of the train of bunches that composes the beam entering in the machine, and ends when the last bunch enters the collider
- acceleration phase, during which the RF cavity provides energy to the beam. This phase ends when the energy of the beam has been ramped up to the one desired for the collisions
- stable beam phase, during which the separation of the beams becomes zero and they are stored in the ring and made to collide in the interaction points, until the quality of the beam is no more useful
- dumping phase, during which a kicker magnet is activated to dump the beam out of the ring in a specifically dedicated location

3.2 Luminosity

The figure of merit of the latter characteristics of a collider is the luminosity $\mathcal{L}$, defined as the proportionality factor between the cross-section σ_p and the rate of events per seconds $\frac{dR}{dt}$, as follows:

$$\frac{dR}{dT} = \mathcal{L}\sigma_p \tag{3.2.1}$$

The unit of measure of luminosity is thus $m^{-2}s^{-1}$, but it is more commonly indicated in $fb^{-1}s^{-1}$or "inverse femtobarns per second", where $1b = 10^{-28}m^2$ and $1fb = 10^{43}m^2$are the popular units to measure the cross section. The luminosity describes the ability of the collider to produce the required number of useful interactions or events, and as it is a relativistic invariant independent of the physical reaction, it is a reliable figure of merit and procedures have been and are being developed to compute and measure it accurately.

3.2.1 Luminosity model

In a collider the beams that circulate are "bunched", meaning each beam is composed of n_b bunches of particles, with a regular spacing between them. So in a multi-bunch beam, we define the total luminosity as

$$\mathcal{L} = n_b f L \tag{3.2.2}$$

where f is the revolution frequency and L is the single bunch crossing luminosity.

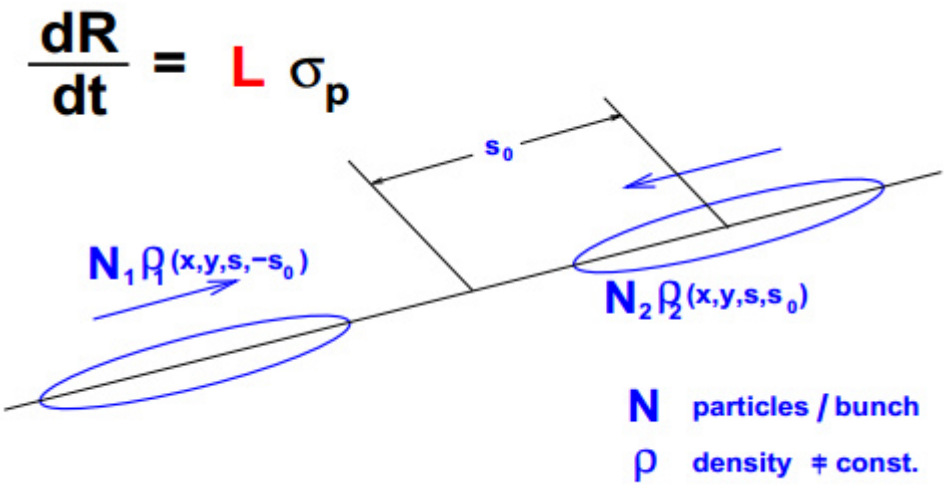

Figure 3.2.1: Single bunch head-on collision scheme[23]

For any two bunches crossing each other in an interaction point (IP), given

- the number of particles N_i contained in each beam i
- the charged particles density distribution in space and time $\rho_i(x, y, s, t)$ of each bunch
- the bunches velocities $\vec{v}_i$

we can compute the single crossing luminosity as

$$\mathcal{L} \propto K N_1 N_2 \int_{-\infty}^{\infty}\int_{-\infty}^{\infty}\int_{-\infty}^{\infty}\int_{-\infty}^{\infty} \rho_1(x,y,z,t)\rho_2(x,y,z,t)dxdydsdt \tag{3.2.3}$$

where K is the kinematic factor

$$K = \sqrt{(\vec{v}_1 - \vec{v}_2)^2 - (\vec{v}_1 \times \vec{v}_2)^2/c^2} \tag{3.2.4}$$

To compute the integral, we can make the simplifying assumption of uncorrelated densities in all planes, thus being able to factorise the density distribusion as

$$\rho_i(x, y, s, t) = \rho_{x_i}(x)\rho_{y_i}(y)\rho_{s_i}(s \pm v_i t) \tag{3.2.5}$$

In principle to calculate the exact value of luminosity we should know each bunch-per-bunch charge distribution. In practice, a Gaussian distribution is in general a good approximation and widely used for analytic calculation. To further reduce the complexity of the problem we make the reasonable assumption that the dispersion is zero at the IP. With these hypotheses, the single bunch distribution will be

$$\rho_i(x, y, s, t) = \frac{1}{(2\pi)^{3/2}\sigma_{x_i}\sigma_{y_i}\sigma_{s_i}} \exp\left(-\frac{x^2}{2\sigma_{x_i}^2} - \frac{y^2}{2\sigma_{y_i}^2} - \frac{(s - v_i t)^2}{2\sigma_{s_i}^2}\right) \quad i = 1, 2 \tag{3.2.6}$$

where σ is the standard deviation of the distribution, that can be calculated as the second order momentum of (2.6.1) in the transverse plane, yielding

$$\sigma_z = \sqrt{\epsilon_z \beta_z} \quad z = x, y \tag{3.2.7}$$

As we are considering high energy bunches, we assume $v_1 = v_2 = c$ and putting together all the above elements, we can rewrite (3.2.2) as

$$\mathcal{L} = \frac{n_b f K N_1 N_2}{(2\pi)^{6/2}\sigma_{x_i}^2\sigma_{y_i}^2\sigma_{s_i}^2}\int_{-\infty}^{\infty}\exp\left(-\frac{x^2}{\sigma_{x_1}^2+\sigma_{x_2}^2}\right)dx\int_{-\infty}^{\infty}\exp\left(-\frac{y^2}{\sigma_{y_1}^2+\sigma_{y_2}^2}\right)dy\int_{-\infty}^{\infty}\exp\left(-\frac{s^2}{\sigma_{s_1}^2+\sigma_{s_2}^2}\right)ds\int_{-\infty}^{\infty}\exp\left(-\frac{(ct)^2}{\sigma_{s_1}^2+\sigma_{s_2}^2}\right)dt \tag{3.2.8}$$

We solve the integrals using the formula

$$\int_{-\infty}^{\infty}\exp\left(-at^2\right)dt = \sqrt{\frac{\pi}{a}} \tag{3.2.9}$$

and in the hypotheses of $\sigma_{s_1} \approx \sigma_{s_2}$ we finally obtain

$$\mathcal{L} = \frac{n_b f K N_1 N_2}{4\pi\sqrt{\sigma_{x_1}^2+\sigma_{x_2}^2}\sqrt{\sigma_{y_1}^2+\sigma_{y_2}^2}} \tag{3.2.10}$$

In the case that the beams have also equal transverse sizes, meaning

$$\sigma_{x_1} = \sigma_{x_2} = \sigma_x \ \cup \ \sigma_{y_1} = \sigma_{y_2} = \sigma_y \tag{3.2.11}$$

then the luminosity for equal beams is expressed as

$$\mathcal{L} = \frac{n_b f K N_1 N_2}{8\pi\sigma_x\sigma_y} \tag{3.2.12}$$

3.2.2 Ideal head-on collision

If the beams are colliding whithout any tilt, then $\vec{v}_1 = -\vec{v}_2$ and thus the kinetic factor becomes $K = 2$, yielding a luminosity factor of

$$\mathcal{L} = \frac{n_b f N_1 N_2}{4\pi\sigma_x\sigma_y} = \mathcal{L}_0 \tag{3.2.13}$$

for equal beams.

3.3 Non-idealities in real machines

In practice we have to include additional effects in our luminosity computations, such as:

- Crossing angles, which are often used to avoid unwanted collisions in machines with many bunches, to minimize data pile-up in the detectors.
- Collision offset, which can be wanted or induced by beam-beam effects
- Hourglass effect, a geometrical effect due to the dependence of the betatron function on the longitudinal position, thus violating our previous assumption of uncorrelated beam parameters
- Non-gaussian beam profiles, whose impact is limited thanks to the central limit theorem.

- Non-zero dispersion at collision point
- $\alpha* \neq 0$ if due to optical imperfections the collision point is not at the waist of the betatron function but slightly displaced, with implications for the effective beam size

The next sections will analyse in more details the first non-idealities in the above list.

3.3.1 Crossing angle

In a collider in general two counterrotating bunches cross each other with a crossing angle ϑ, as shown in Figure 3.2. This is not only motivated by technical reasons but also allows to contain destructive effects on the beam, the so-called long range beam beam effects that will be analysed in the next chapter. It is the relative size of the total beam separation, measured in units of the beam size σ, that is the relevant parameter when evaluating the impact of parasitic beam-beam collisions. On the other hand the crossing angle reduces the luminosity: the larger is the crossing angle, the smaller is the area of overlap ant therefore smaller is the possibility of collision between two hadrons.

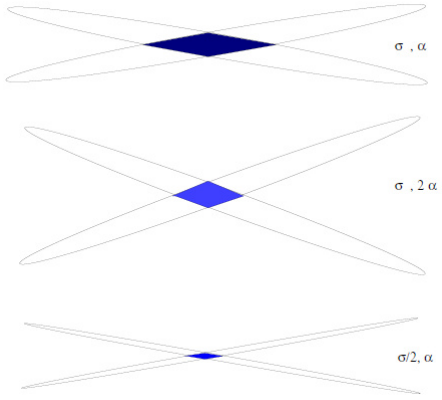

Figure 3.3.1: Schematic of the luminous region, depending on the crossing scheme[24].

Assuming a crossing in the horizontal plane (x,s), the new coordinates, shown in (3.3.2), become

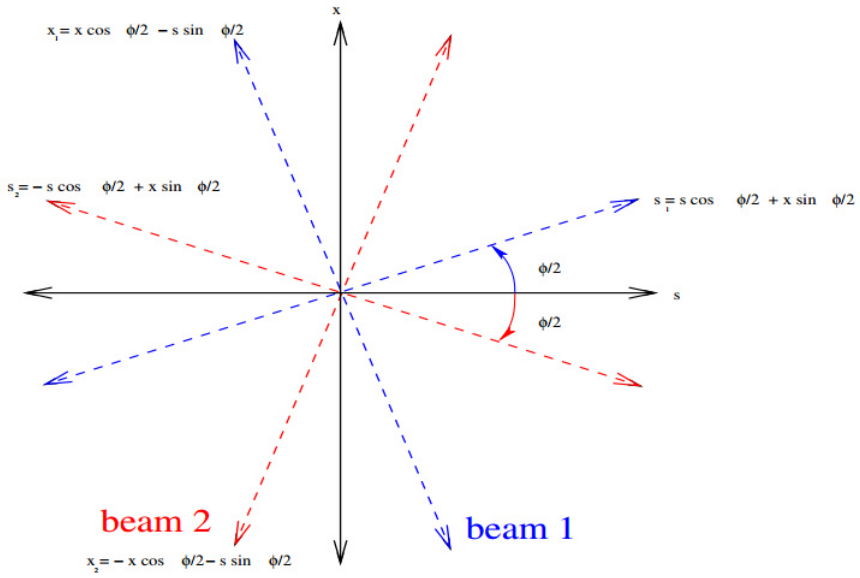

Figure 3.3.2: Tilted coordinates for the crossing angle collision scheme[23]

$$\begin{cases} x_1 = x\cos\frac{\phi}{2} - s\sin\frac{\phi}{2}, & s_1 = s\cos\frac{\phi}{2} + x\sin\frac{\phi}{2} \\ x_2 = x\cos\frac{\phi}{2} + s\sin\frac{\phi}{2}, & s_2 = s\cos\frac{\phi}{2} - x\sin\frac{\phi}{2} \end{cases} \tag{3.3.1}$$

Moreover, the kinematic factor changes, as the velocities of the opposing beam now are not parallel anymore, thus yielding

$$K_{ca} = 2\cos^2\frac{\phi}{2} \tag{3.3.2}$$

Taking into account the above considerations, the luminosity expression for equal beams becomes

$$\mathcal{L} = 2\cos^2\frac{\phi}{2} N_1 N_2 f n_b \int_{-\infty}^{\infty}\int_{-\infty}^{\infty}\int_{-\infty}^{\infty}\int_{-\infty}^{\infty} \rho_{x_1}(x_1)\rho_{y_1}(y_1)\rho_{s_1}(s_1 - s_0)\rho_{x_2}(x_2)\rho_{y_2}(y_2)\rho_{s_2}(s_2 + s_0)dxdydsdt \tag{3.3.3}$$

To solve the integral in the case of two identical gaussian round beams, we now use not only (3.2.9) but also formula

$$\int_{-\infty}^{\infty} \exp[-(at^2 + bt + c)]dt = \sqrt{\pi/a}\cdot\exp\left(\frac{b^2 - ac}{a}\right) \tag{3.3.4}$$

Moreover, we neglect all the mixed product terms of σ_x, x *and* $sin(\phi/2)$ and approximate the latter term with the tangent, in the realistic hypotheses of small crossing angle. Finally, luminosity can be expressed as

$$\mathcal{L} = \frac{N_1 N_2 f n_b}{4\pi\sigma_x\sigma_y}\cdot S = \mathcal{L}_0 \cdot S \tag{3.3.5}$$

where S is the *reduction factor* due to crossing angle and can be expressed as

$$S = \frac{1}{\sqrt{1 + (\frac{\sigma_s}{\sigma_x}\tan\frac{\phi}{2})^2}} \approx \frac{1}{\sqrt{1 + (\frac{\sigma_s}{\sigma_x}\frac{\phi}{2})^2}} \tag{3.3.6}$$

in the usual case of $\sigma_s \gg \sigma_{x,y}$. The quantity $\theta_{PA} = \frac{\phi\sigma_s}{2\sigma_x}$ is called the *Piwinski angle*.

3.3.2 Offset

It is possible to have the beams cross not only with a crossing angle, but also with an offset distance between the two beam centroids in the crossing plane. The coordinates in which is more convenient to analyse the interaction are thus

$$\begin{cases} x_1 = d_1 + x\cos\frac{\phi}{2} - s\sin\frac{\phi}{2}, s_1 = s\cos\frac{\phi}{2} + x\sin\frac{\phi}{2} \\ x_2 = d_2 + x\cos\frac{\phi}{2} + s\sin\frac{\phi}{2}, s_2 = s\cos\frac{\phi}{2} - x\sin\frac{\phi}{2} \end{cases} \tag{3.3.7}$$

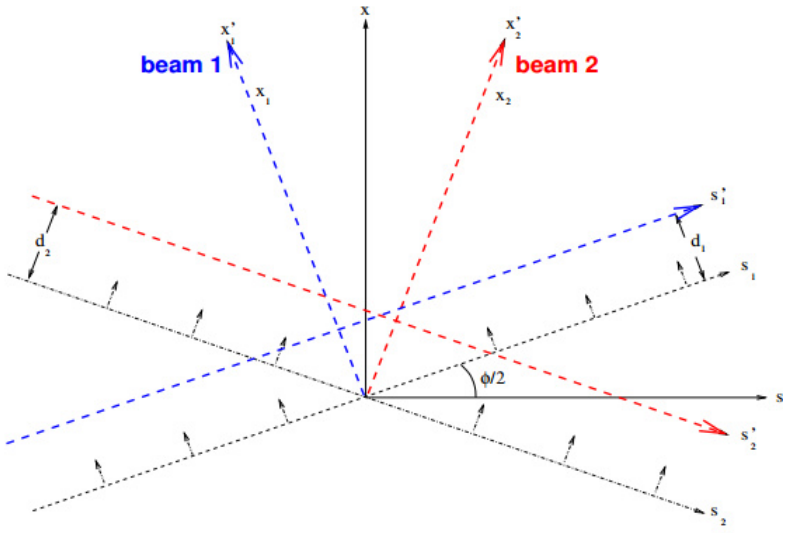

Figure 3.3.3: New axes for a collision with crossing angle and beams offset[23]

So we need to solve (3.3.3) with the new coordinates. After integration in dy and ds_0, which are unchanged, the new integral yields

$$\begin{gathered} \mathcal{L} = \frac{N_1 N_2 f n_b}{2\pi\sigma_x\sigma_s} \cdot 2\cos^2\frac{\phi}{2} \int\int \exp\left(-\frac{x^2\cos^2\frac{\phi}{2} + s^2\sin^2\frac{\phi}{2}}{\sigma_x^2}\right) \\ \exp\left(-\frac{x^2\sin^2\frac{\phi}{2} + s^2\cos^2\frac{\phi}{2}}{\sigma_s^2}\right) \exp -\left(-\frac{d_1^2 + d_2^2 + 2(d_1+d_2)x\cos\frac{\phi}{2} - 2(d_2-d_1)s\sin\frac{\phi}{2}}{\sigma_x^2}\right) dxds \end{gathered} \tag{3.3.8}$$

Integrating over x, we then obtain

$$\mathcal{L} = \frac{N_1 N_2 f n_b}{8\pi^{\frac{3}{2}}\sigma_s} \cdot 2\cos^2\frac{\phi}{2} \int W \cdot \frac{\exp(-As^2 + 2Bs)}{\sigma_x\sigma_y} ds \tag{3.3.9}$$

where

$$\begin{gathered} A = \frac{\sin^2\frac{\phi}{2}}{\sigma_x^2} + \frac{\cos^2\frac{\phi}{2}}{\sigma_s^2} \qquad B = \frac{(d_2-d_1)\sin\frac{\phi}{2}}{2\sigma_x} \\ W = \exp\left[-\frac{1}{4\sigma_x^2}(d_s - d_1)^2\right] \end{gathered} \tag{3.3.10}$$

In conclusion, when there are a crossing angle and an offset between the beams, the luminosity formula becomes

$$\mathcal{L} = \mathcal{L}_0 \cdot W \cdot S \cdot \exp(\frac{B^2}{A}) \tag{3.3.11}$$

where S depends on the crossing angle ϕ, W depends on the offset separation d and the exponential term depends on both phenomena.

Chapter 4

Beam-beam interaction at high energy

Thus far we have considered only the motion of a beam of non interacting particles in the presence of external forces. Many of the interesting phenomena in accelerator physics involve the dynamic interplay between the beam and its surroundings through the electromagnetic fields initiated by the beam. Usually, the consequences are not benign and there is a catalog of beam instabilities analogous to the ones of hydrodynamics. Among the effects for which the intensity of the beam is important, we are particularly interested in the study of the so called beam-beam effect.

The two counterrotating beams in the LHC circumference are made to collide in four interaction points, where they pass each other in the common beam and are subject to each other electromagnetic fields. As the two beams share one common beam pipe around the four designed interaction points, the protons will suffer up to 120 additional long-range or "parasitic" collisions with bunches of the opposing beam. The effect of these long range collisions limits the dynamic stability of the protons and will likely reduce the beam lifetime.

This mechanism causes abrupt changes in the particle phase space distribution, resulting in a larger than desired phase space area demanded by the beam.

A beam acts on particles like an electromagnetic lens, but it does not represent a simple form (i.e. not well defined multipoles). Instead it presents a very non-linear form of the forces, depending on the charge density distribution within the single bunch, which can vary from bunch to bunch. Moreover, the result of the interaction between the beams is a change in the charge density distribution itself.

The beam-beam force is one of the most important limiting factors in the performance of a collider, mainly in the delivered luminosity. For high bunch intensities the beam-beam force is strong enough to expect orbit effects if the two beams do not collide head-on but with a crossing angle or with a given offset.

4.1 Interaction region

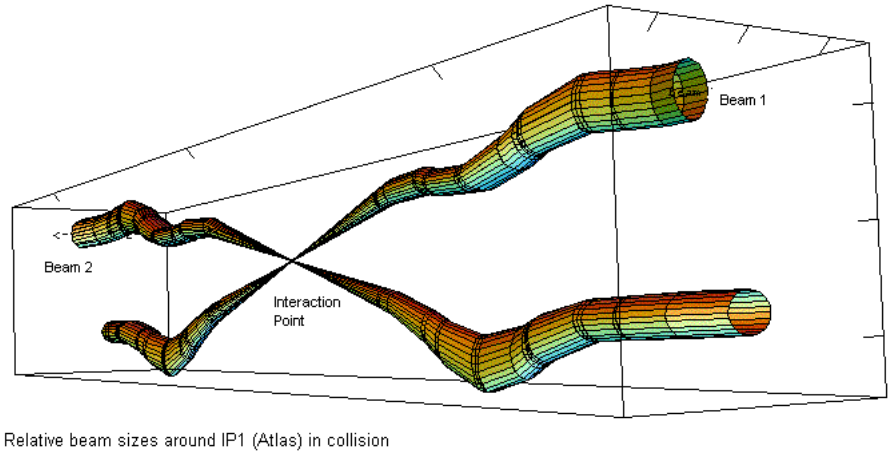

Figure 4.1.1: Tridimensional representation of the beams envelopes at IP1(ATLAS)[5].

In the LHC two proton beams, each composed of 2808 bunches with 10^{11}average number of protons per bunch, are stored in two separate beam pipes in counterrotating orbits. Then, in 4 interaction regions (IRs) the beam separation is reduced via the activation of individually powered dipoles, until the two opposing beams collide at the center of the interaction region, in the interaction point (IP).

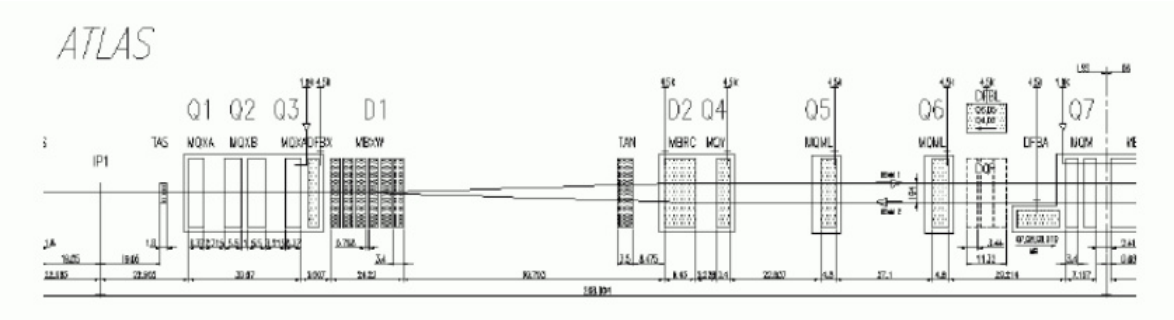

Figure 4.1.2: Schematic of the optics in the interacion region around IP1. From left to right: (Q1,Q2,Q3) final triplet quadrupoles; D1: dipole separator; TAN: Target Absorber; remaining elements: matching magnets.

4.2 Beam-beam interaction at a glance

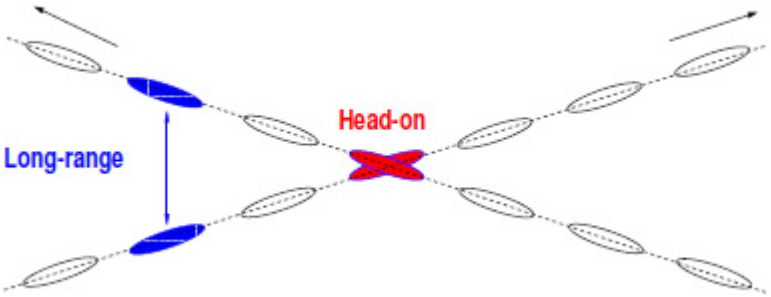

Figure 4.2.1: Schematic of the behaviour of bunched beams in the LHC interaction regions[25]

The beam-beam force arises from the fact that when the two colliding charged beams pass each other in the common beam pipe next to the interaction points (IPs), they exert a force on one another.

We can distinguish two kind of phenomena:

- Head-On beam-beam interaction (HO), occurring when the counterrotating bunches cross each other with their center transversely aligned (without offset and without crossing angle);
- Long Range Beam-Beam Interactions (LRBBI), which occur at a large transverse offset compared with the beam size, before and after the collision point.

In both cases the parasitic interaction mostly causes localised periodic distortions, which can cause instability in the betatron oscillations, corresponding to a tune shift in the frequency space, as we will present in the next paragraph. Furthermore, as a result of the interaction, the charge distribution can change, which has strong implications for fields and forces.

While the head-on collision is unavoidable, the number and the strength of long-range interaction depends on the design parameters (crossing angle, bunch spacing, optics layout).

We will first present the model for the head-on beam beam effect, and in the analysis we will consider the interaction of a single particle of one beam interacting with the electromagnetic field generated by the other beam (weak-strong model).

4.3 Head-on beam-beam force

The transverse force exerted on a particle with velocity $\vec{v_1}$ from a counter-rotating bunch that moves with velocity $\vec{v_2}$ is the Lorentz force

$$\vec{F}=\mathrm{e}(\vec{E}+\vec{v_1}\times\vec{B}) \tag{4.3.1}$$

In the particle rest frame we only have electrostatic fields, i.e. $\vec{E'}\neq 0$, $B'\vec{\equiv}0$. Transforming the fields into the laboratory frame through Lorentz transformations we obtain:

$$\begin{array}{cc} E_\parallel = E'_s & B_\parallel = \frac{\gamma_2}{c^2}\vec{v}_2\times E'_\parallel = 0 \\ E_\perp = \gamma_2 E'_\perp & B_\perp = \frac{\gamma_2}{c^2}\vec{v_2}\times E'_\perp \end{array} \tag{4.3.2}$$

We are interested in the transverse component of the force that one beam exerts on the other, which depends only on the transverse components of the fields, thus being

$$F_\perp = e\gamma_2 E'_\perp(1+\beta_1\beta_2) = eE_\perp(1+\beta_1\beta_2) \tag{4.3.3}$$

where $\beta_i = \frac{v_i}{c}$ for $i = 1, 2$.

We only need to know the transverse component of the electrostatic field in the rest frame of the beams to compute the final value of the force.

To obtain such value, we first calculate the electromagnetic potential satisfying Poisson equation

$$\nabla^2\phi = -\frac{1}{\epsilon_0}\rho(x,y,s) \tag{4.3.4}$$

whose general solution in polar coordinates is

$$\phi(\vec{r}) = \frac{1}{4\pi\epsilon_0}\int\frac{\rho(\vec{r'})}{|\vec{r}-\vec{r'}|}d^3\vec{r'} \tag{4.3.5}$$

and finally deriving the electric field as its gradient

$$\vec{E'} = -\nabla\phi(x,y,s) \tag{4.3.6}$$

The field is obtained by integrating over the charge distribution, which can follow various possible functions, leading to different fields (and thus forces). It is not always possible to integrate the distribution to arrive at an analytical expression for the forces, in which case either approximation or numerical methods have to be used.

4.3.1 Beam-beam force for a Gaussian beam

As the bunch length is much bigger than the transverse size of the beam, i.e. $\sigma_s \gg \sigma_{x,y}$, we can neglect the contribution of the longitudinal extension of the bunch to the gaussian charge density. Thus we assume it to be a bi-Gaussian distributions $\rho(x,y) = \rho(x)\rho(y)$ in the transverse planes

$$\rho(x,y) = \frac{ne}{\sigma_x\sigma_y 2\pi}exp\left(-\frac{x^2}{2\sigma_x^2}-\frac{y^2}{2\sigma_y^2}\right) \text{ where } z = x,\, y \tag{4.3.7}$$

with

$$\sigma_z = \sqrt{\beta_z \epsilon_z} \qquad \text{with } z = x, y \tag{4.3.8}$$

Plugging (4.3.7) into (4.3.4), we can give the potential close expression as [20]

$$\phi(x,y) = \frac{ne}{4\pi\epsilon_0} \int_0^\infty \frac{exp\left(-\frac{x^2}{2\sigma_x^2+q} - \frac{y^2}{2\sigma_y^2+q}\right)}{\sqrt{(2\sigma_x^2+q)(2\sigma_y^2+q)}} dq \tag{4.3.9}$$

where n is the number of particles in a bunch, e is the elementary charge and ϵ_0 is the permittivity of free space. It can be demonstrated that this formula satisfies the potential by plugging it back into Poisson's equation.

4.3.2 Round beams approximation

When the two beams are brought into collision, they are usually made round meaning $\sigma_x \approx \sigma_y \approx \sigma$. With this simplifying assumption, (4.3.9) becomes

$$\phi(r) = \frac{ne}{4\pi\epsilon_0} \int_0^\infty \frac{\exp\left(-\frac{r^2}{2\sigma^2+q}\right)}{(2\sigma^2+q)} dq \tag{4.3.10}$$

where $r^2 = x^2 + y^2$. Now it is more convenient to obtain the transverse electric field in cylindrical coordinates, as

$$E_r = \frac{ne}{4\pi\epsilon_0} \frac{\delta}{\delta r} \int_0^\infty \frac{\exp\left(-\frac{r^2}{2\sigma^2+q}\right)}{(2\sigma^2+q)} dq \tag{4.3.11}$$

The integral can be solved by changing the integration variable from q to $t = \frac{1}{2\sigma^2+q}$ and inverting the order of integration and differentiation.

$$E_r = \frac{ne}{2\pi\epsilon_0} r \int \exp(-tr^2)dt = -\frac{ne}{2\pi\epsilon_0} \frac{1}{r} \left[1 - \exp(-\frac{r^2}{2\sigma^2})\right] \tag{4.3.12}$$

The final step to obtain the expression of the force in cylindrical coordinates is trivially to multiply the field by the factor $e(1+\beta_1\beta_2)$ as in (4.3.3). In the collision point we assume the two beams to be travelling with the same β, finally obtaining

$$F_r = -\frac{ne^2(1+\beta^2)}{2\pi\epsilon_0} \frac{1}{r} \left[1 - \exp(-\frac{r^2}{2\sigma^2})\right] \tag{4.3.13}$$

As we want to analyse the dynamics along each transverse axis separately, we decompose the radial force into its components, obtaining

$$\begin{aligned} F_x &= -\tfrac{ne^2(1+\beta^2)}{2\pi\epsilon_0} \tfrac{x}{r^2} \left[1 - \exp(-\tfrac{r^2}{2\sigma^2})\right] \\ F_y &= -\tfrac{ne^2(1+\beta^2)}{2\pi\epsilon_0} \tfrac{y}{r^2} \left[1 - \exp(-\tfrac{r2}{2\sigma^2})\right] \end{aligned} \tag{4.3.14}$$

Thus we see that the head-on beam-beam force is defocusing in both degrees of freedom for like-sign beams. All we have derived so far is relative to the force of a beam on a single test particle. It can be used to study single particle or

incoherent effects, treating a particle crossing a beam like it was moving through a static electromagnetic lens. We would like to go one step further and obtain the value of the "kick", i.e. the change of the slope of the particle trajectory, that a single particle experiences while crossing a round beam of finite length (weak-strong approach). To do this, we start from the two-dimensional force and multiply it by the longitudinal distribution, which depends on both position s and time t, assuming it also has a Gaussian shape with a standard deviation of σ_s:

$$F_r(r,s,t) = -\frac{ne^2(1+\beta^2)}{(2\pi)^{3/2}\epsilon_0}\frac{1}{r}\left[1-\exp(-\frac{r^2}{2\sigma^2})\right]\left[\exp(-\frac{(s+vt)^2}{2\sigma_s^2})\right] \tag{4.3.15}$$

Using the kick definition and integrating Newton's equation we obtain

$$\Delta r' = \frac{p_x}{p_0} = \frac{\int F(r,s,t)dt}{m\gamma\beta c} = -\frac{2Nr_0}{\gamma}\frac{1}{r}\left[1-\exp(-\frac{r^2}{2\sigma^2})\right] \tag{4.3.16}$$

where N is the number of parasitic interactions and while we have rewritten the constant multiplication factor in terms of the classical particle radius

$$r_0 = \frac{1}{4\pi\epsilon_0}\frac{e^2}{mc^2} \tag{4.3.17}$$

Again projecting the kick on the transverse axes we obtain the Cartesian coordinates of the transvers kicks as

$$\begin{aligned}\Delta x' &= -\tfrac{2Nr_0}{\gamma}\tfrac{x}{r^2}\left[1-\exp(-\tfrac{r^2}{2\sigma^2})\right]\\ \Delta y' &= -\tfrac{2Nr_0}{\gamma}\tfrac{y}{r^2}\left[1-\exp(-\tfrac{r2}{2\sigma^2})\right]\end{aligned} \tag{4.3.18}$$

where N is the total number of particles in the opposing bunch.

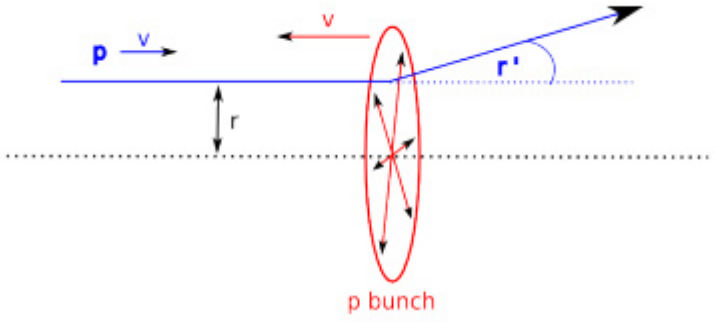

Figure 4.3.1: Incoming particle is deflected (kicked) by the beam-beam force of the opposing beam[16]

4.3.3 Linear beam-beam tune shift

The focal lenght of the lens associated with the beam-beam effect, in the asymptotic limit, is

$$\Delta r'|_{r\to 0} = -\frac{Nr_0 r}{\gamma} = r\cdot f$$

so we can approximate the beam-beam effect as an additional defocusing quadrupolar term.

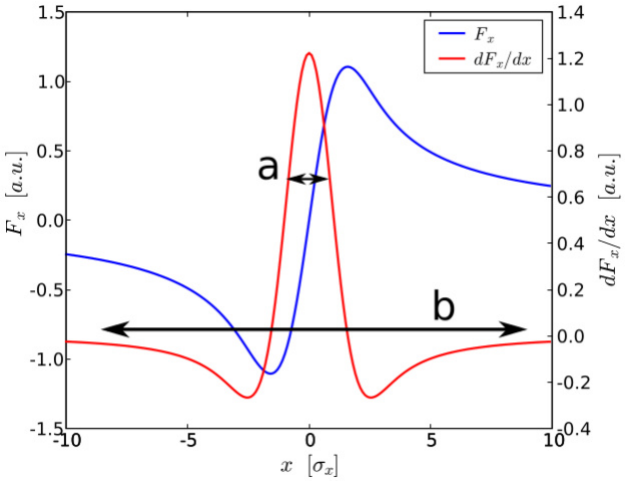

Figure 4.3.2: Red: head-on beam-beam force versus particle amplitude in r.m.s. beam size; Blue: beam-beam force derivative versus particle amplitude in r.m.s. beam size[23]

Figure 4.3.2 shows the dependence of the kick on the dispacement of the particle from the center of the opposing bunch. Due to symmetry, zero-amplitude particles do not experience any kick. Near the center of the bunch, the kick is similar to that of a quadrupole; further away it becomes non-linear. As the kick strength vanishes for higher amplitudes, the head on collision itself cannot cause beam loss. As the effect of the linear part of thebeam-beam interaction is equivalent to that of a focusing error, it is useful to describe the effect on the opposite beam by a tune shift, as any quadrupole error with strength δk and lenght Δs causes a tune shift of

$$\Delta\nu_y = \frac{1}{4\pi}\int \beta_y(s)\delta k_y(s)ds = \frac{1}{4\pi}\int \beta(s)\frac{\partial F_y}{\partial y}ds \tag{4.3.19}$$

We can calculate the value of the linear tuneshift for a small amplitude particle in the (a) region at the collision point, called the beam-beam parameter, as

$$\xi = \frac{r_0\beta*}{4\pi\gamma\sigma^2} \tag{4.3.20}$$

where $\beta*$ is the optical amplitude function at the IP.

ξ is also called the beam-beam parameter, as it gives a measure of the detuning to to beam-beam interaction. The following table contains the values needed to calculate it for the nominal LHC.

Parameter	Nominal LHC
Energy	7 TeV
Intensity	$1.15 \cdot 10^{11}$/bunch
Beam size $\sigma_x \cdot \sigma_y (in\ IP1\&IP5)$	$16\mu m \cdot 16\mu m$
Beta function $\beta_x \cdot \beta_y$	$0.55\,m \cdot 0.55$
Crossing angle	$285\mu rad$
Beam-beam parameter	0.0037

Table 4.3.1: Beam beam parameter calculation for the nominal LHC

4.4 Long-range beam-beam force

If the bunches do not collide head-on but with a transverse offset large compared with the beam size, the electromagnetic interaction is referred to as long-range beam-beam interaction.

The total number of long-range interactions can be computed from the bunch spacing and the length of the common path. The space structure of the parasitic collisions depends on the precise location of the separation dipoles and with the current layout the calculation yields 14-15 encounters on each side of each IP.

The kick due to a single LRBBI can be derived from 4.3.18 by a simple coordinate transformation $z = z + d$ where $z = x, y$ and d is the separation between the beams.

As a practical example, let's analize the case in which we have round beams and a vertical crossing angle. The long-range beam-beam kick becomes

$$\begin{aligned} \Delta x' &= -\frac{2Nr_0}{\gamma}\frac{x}{r^2}\left[1 - \exp(-\frac{r^2}{2\sigma^2})\right] \\ \Delta y' &= -\frac{2Nr_0}{\gamma}\frac{(y+d)}{r^2}\left[1 - \exp(-\frac{r2}{2\sigma^2})\right] \end{aligned} \tag{4.4.1}$$

where $r = \sqrt{x^2 + (y-d)^2}$.

It is fairly obvious that the effect of long-range interactions must strongly depend on the separation.

The normalised separation between the beams can be calculated as

$$\frac{d}{\sigma} \approx \frac{\theta_c}{\sigma'_y} \tag{4.4.2}$$

where θ_c is the full crossing angle and σ'_y is the beam vertical divergence. For large separation $d \gg 6\sigma$, as in the case of the LHC, the exponential term becomes small and the kick can be approximated as

$$\Delta y' = -\frac{2Nr_0}{\gamma}\frac{(y+d)}{r^2}\left[1 - \left(1 - \frac{r^2}{2\sigma^2} + O(r^4)\right)\right] = \frac{Nr_0}{\gamma\sigma^2}(y+d) + O(r^2) \tag{4.4.3}$$

This shows a constant contribution to the beam-beam kick which acts as a closed orbit kick as it has a component that is independent of the particle's betatron amplitude or momentum.

The normalised separation d/σ is provided by the small crossing angle θ_c as

$$\frac{d}{\sigma} \approx \frac{\theta_c}{\sigma'} = \frac{\theta_c}{\sqrt{\epsilon/\beta*}} \tag{4.4.4}$$

The calculation shows that the linear tune spread from long-range interactions alone follows an approximate scaling of

$$\Delta\nu_y \propto \frac{N}{d^2} \tag{4.4.5}$$

This transformation results in a non-zero kick for zero amplitude particles and thus in a changed closed orbit and it breaks the symmetry between the two planes. Static orbit correctors and choosing alternate crossing planes (horizontal-vertical),

as actually is done in LHC, helps in reducing the long-range effect. From the IP to the first quadrupole, the normalized beam-beam separation is constant and fixed by the crossing angle and $\beta*$. The triplet affects the two beams and thus each of its quadrupoles focuses one beam in one plane while defocusing the other beam in the other plane, respectively. Figure shows the symmetry breaking in the tune diagram.

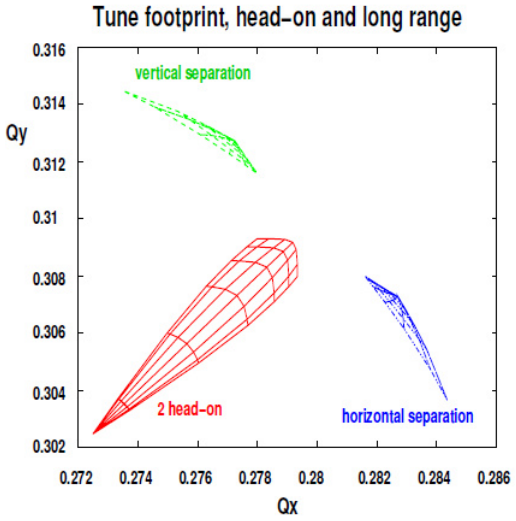

Figure 4.4.1: Foot print for two proton-proton head-on interactions (red), long-range interactions in the horizontal plane (blue) and long-range interactions in the vertical plane (green).

4.4.1 LHC Filling scheme

In the nominal design, the LHC ring is filled with bunch trains consisting of 72 bunches with 25ns spacing. Two trains are interleaved with gaps of varying length, as summarised in figure (4.4.2). Therefore bunches at the end of a bunch train, so called PACMAN bunches, experience a reduced number of LRBBIs. The extreme bunches at the very end of the train experience no LRBBI at all at one side of the IP. As a result these bunches have different orbits and tunes.

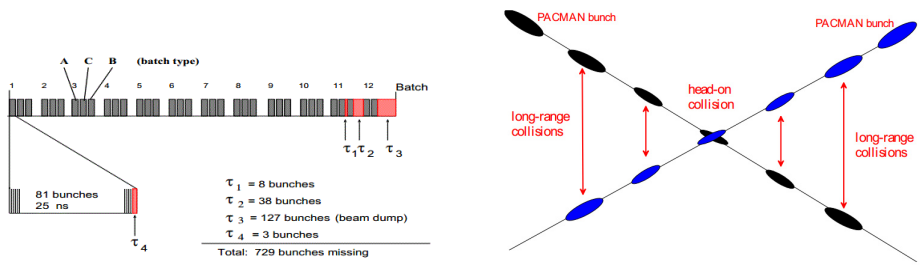

Figure 4.4.2: LHC filling scheme and PACMAN long-range interaction scheme[23]

Chapter 5

Simulation tools

To obtain our goal of studying the evolution of distributions at the LHC interaction points, we need to use simulations tools that implement the effect of the electromagnetic elements of the accelerator and of the beam. We use two of such tools, which have been developed at CERN and are integrated and optimized for tracking studies: MAD-X, an optics code, and SixTrack, a tracking code. This chapter will present their respective features and what are the main parameters used for our simulations.

5.1 MADx

The MAD-X (Methodical Accelerator Design) program is a general purpose accelerator and lattice design program.

It is used to design the optics of accelerators. To do so, it is capable of calculating the optics parameters from a machine description, given in terms of single elements properties (e.g. dipole field strength), and to match them to the desired properties of such machine. Finally it is also capable of simulating the beam dynamics in the designed machine. Both, circular and linear accelerators (or beam lines) are normally handled by such program.

The design of a machine requires the definition of the machine and the basic ingredients are:

- definition of the properties of all machine elements
- strength of all active machine elements
- position of all machine elements in the machine i.e. the order in which they appear in the accelerator or beam line

These definitions are enabled by a well adapted and defined input language. MAD is a project aiming to be at the forefront of computational physics in the field of particle accelerator design and simulation. The MAD scripting language is de facto the standard to describe particle accelerators and optimize beam optics.

The MAD-X input consists of a sequence of statements (commands, actions, or declarations etc.). All statements are free format with "," as separators, can occupy any number of lines and are terminated by a semicolon ";".

5.1.1 Machine description

For the calculations, the elements can be defined as

- thick lenses with a finite length;
- thin lenses with zero length.

In the latter case, the effects of an element (e.g. a magnet) on the beam are represented as impulses (kicks) at a fixed value s on the reference orbit. This simplifies the treatment since it allows to treat the machine as a series of linear transformations separated by the "kicks" at the positions of the thin elements. This method is very fast and symplectic by construction and it is therefore best suited for particle tracking. The disadvantage is the loss of precision when the magnets are very long (compared to the size of the machine) or when fringe fields are important. Part of this precision can be recovered by sub-dividing the magnets into slices, i.e shorter sections, each representing a thin lens. A special class of elements of MADx is the MULTIPOLE one. With this, the user can specify the normal and skew components of the multipole ()multiplied by the relevant magnetic length (KNL and KSL). Note that the strength definitions are position dependent. The attribute LRAD is a fictitious length, which is only used to compute synchrotron radiation effects.Using multipoles, a thin quadrupole can be defined as:

```
QFT: MULTIPOLE, LRAD=0, KNL={0, kn1L, 0, 0};
```

The representation of the machine is called a sequence. It defines the order in which the elements appear in the accelerator or beam line.

The sequence of a periodic machine or the periodic part of a machine can be defined using the MAD-X macro commands. After the usual definition of the cell length *lcell*, the half length of a quadrupole *lquad* and the number of cells *ncell*, the whole machine can be defined with a while-loop.

In addition to the statements which are used to define a machine, the MAD-X commands are used to define and execute actions on the machines, e.g. calculations of Twiss functions, I/O of the lattices, particle tracking etc.

At the end of the execution of a TWISS command, to calculate the twiss value, a summary table is printed, containing the following information

parameter	corresponding variable
Accelerator's circumference	length
Closed Orbit	orbit5
Momentum compaction factor	alfa
Transverse Relativistic Gamma Factor	gammatr
Horizontal Tune	q1
Horizontal Detuning	dq1
Maximum Horizontal Beta Function	betxmax
Maximum Horizontal Dispersion	dmax
R.m.s. Dispersion	dxrms
Max Horizontal Covariance	xcomax
R.M.S. Horizontal Covariance	xcorms
Vertical Tune	q2
Vertical Detuning	dq2
Maximum Vertical Beta Function	betymax
Maximum Vertical Dispersion	dymax
R.m.s. Dispersion	dyrms
Max Vertical Covariance	ycomax
R.M.S. Vertical Covariance	ycorms
Longitudinal Momentum Spread	deltap

Table 5.1.1: Summary table physical parameters and their corresponding variables names in MADx

During the design process of a machine it becomes important to test it against imperfections. For that purpose, alignment and field errors can be assigned to all machine elements. The calculations will take these imperfections into account. The program allows to assign field errors of any order to the machine elements.

5.2 SixTrack

SixTrack, a 6D single particle symplectic tracking code developed at CERN to perform particle-tracking studies and predict the beam behaviour through evaluation of the particle trajectory along the lattice optics. It is optimized for long term tracking (>100 000 turns) in high energy rings. It is mainly used for the LHC for dynamic aperture studies, tune optimization and collimation studies. SixTrack has produced results that are essential for veryfying the long term stability of the high energy particles in the LHC. For the time being, no theory can predict with sufficient accuracy the long term behaviour of particles in non linear fields, leading to the need to rely on fast computers to track hundreds of particles step by step through the thousands LHC magnets for up to a million turns.

A particle tracking program for accelerators like SixTrack is based on two concepts:

- beamline elements representing real devices (dipoles, quadrupoles, cavities)
- symplectic integrators using predefined maps (i.e. solutions of equations of motion)

A map is a transformation of particle coordinates formulated in such a way that coordinates can be either floating point number or truncated polynomials. A map may reflect the effects of a field on a particle or a charge of the reference frame or other non physical transfomations.
An integrator solves the equations of motion of a particle under the influence of a specific force often generated by electromagnetic fields using some approximations. It is often coded as an explicit map or a sequence of them.
A particle trajectory in beamline element can equally well be computed using different type of integrators depending on the initial conditions and the application.
For relativistic particles an integrator can be qualified in terms of:

- longitudinal coordinate definition (s or t)
- the approximation of the Hamiltonian: exact or expanded
- the type of Hamiltonian splitting:
  - kick-drift
  - matrix-kick: keep the linear motion exact
  - no splitting: solving the motion exactly
- the order of approximation in s
- the integration step inside an element

The features at which we are interested for our tracking studies are the possibility to compute the evolutions of one or more particle trajectories along beamline elements for a large number of turns and the availability of post-processing analysis tools (particle loss, frequency maps, invariant reconstruction, etc.).
In (B) we report the parts of the program's syntax and manual most significant for our goals. In the next paragraphs we will present the concept of six dimensional phase space and how the beam-beam kick is implemented in the simulator.

5.2.1 6D phase space

Tracking in 6D means that the six dimensional phase space is analysed. Phase space is, as discussed in chapter (2), is a space made up of the position and momentum of a particle, which can be plotted together in a phase diagram to highlight the relationship between the quantities. Thus a particle moving in three dimensions has a phase space with six dimensions, that is three degrees of freedom. There are several ways in which one can define the variables to determine such a space. In our discussion, we have always talked in terms of position and divergence rather than momentum, thanks to the paraxial approximation. We consider the general 6D vector in the complete phase space to have the following components:

$$\vec{q} = (x,\, x',\, y,\, y',\, s,\, \frac{\Delta p}{p})$$

For a proton ring, where synchrotron radiation is negligible and in the hypothesis of longitudinal oscillations being much slower than betatron ones, one could even limit the study to the 4D transverse phase space, and SixTrack also offers this flexibility to choose among the two types of simulation.

5.2.2 Beam-beam element

The following section illustrates the tracking maps used by SixTrack, labelled by the beam line elements that the maps approximately represent. The map is the solution of the equations of motion for a step L in the independent parameter s with a given set of initial conditions in the canonical coordinates. High order integrators for single beam line elements can be built by combining simpler maps (e.g. thin kicks and drifts).

Beam beam kick calculation

In the incoherent or weak-strong model, a test particle interacts with the mean field produced by the couter-rotating beam bunch. The stability of the test particle depends essentially on the single particle dynamics. In order to study beam-beam interactions the strong bunch can be split longitudinally into several slices, each slice described by an electrostatic potential of the form already analysed in (4.3.9), presented here again in the beam envelope notation as

$$U(\hat{x},\hat{y};\hat{\Sigma}_{11},\hat{\Sigma}_{33}) = \frac{r_0}{\gamma}\int_0^\infty \frac{\exp\left(-\frac{\hat{x}}{2\hat{\Sigma}_{11}+u}-\frac{\hat{y}}{2\hat{\Sigma}_{33}+u}\right)}{\sqrt{2\hat{\Sigma}_{11}+u}\sqrt{2\hat{\Sigma}_{33}+u}}du \tag{5.2.1}$$

where Σ_{ij} are the elements of the 6x6 phase-space envelop matrix Σ of the strong bunch, which is the covariance matrix of the particles' distribution, defined as

$$\Sigma = \begin{pmatrix} \sigma_{11} & \cdots & \cdots & \cdots & \sigma_{16} \\ \vdots & \ddots & & & \vdots \\ \vdots & & \ddots & & \vdots \\ \vdots & & & \ddots & \vdots \\ \sigma_{61} & \cdots & \cdots & \cdots & \sigma_{66} \end{pmatrix} = \begin{pmatrix} \langle X^2\rangle & \langle XX'\rangle & \langle XY\rangle & \langle XY'\rangle & \langle XZ\rangle & \langle XZ'\rangle \\ \langle XX\rangle & \langle X'^2\rangle & \langle X'Y\rangle & \langle X'Y'\rangle & \langle X'Z\rangle & \langle X'Z'\rangle \\ \langle XY\rangle & \langle X'Y\rangle & \langle Y^2\rangle & \langle YY'\rangle & \langle YZ\rangle & \langle YZ'\rangle \\ \langle XY'\rangle & \langle X'Y'\rangle & \langle Y'^2\rangle & \langle XY'\rangle & \langle Y'Z\rangle & \langle Y'Z'\rangle \\ \langle XZ\rangle & \langle X'Z\rangle & \langle YZ\rangle & \langle Y'Z\rangle & \langle Z^2\rangle & \langle ZZ'\rangle \\ \langle XZ'\rangle & \langle X'Z'\rangle & \langle YZ'\rangle & \langle Y'Z'\rangle & \langle ZZ'\rangle & \langle Z'^2\rangle \end{pmatrix}$$

where we have used the capital letters notation to indicate the strong bunch coordinates.

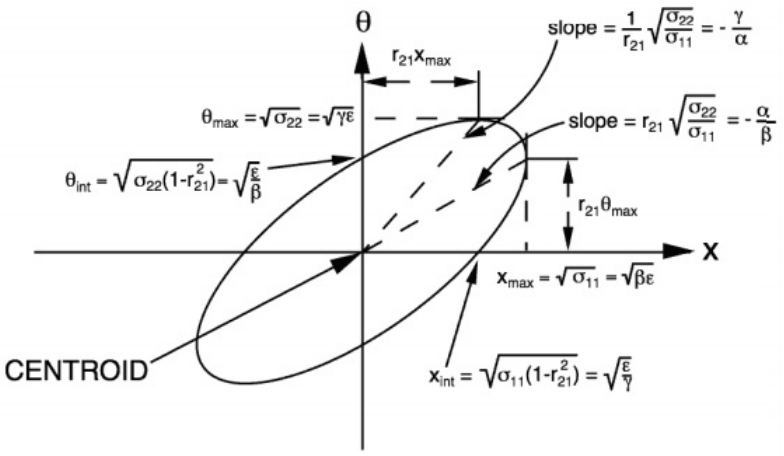

Figure 5.2.1: Strong bunch phase space[2]

For a round beam, this translates into the transverse kick from a beam-beam element being

$$\begin{pmatrix} p_x \to p_x + r_0 \cdot S \cdot \frac{r_x}{r^2} \left[1 - \exp(\frac{r^2}{2\sigma^2})\right] - d_{offset_x} \\ p_y \to p_y + r_0 \cdot S \cdot \frac{r_y}{r^2} \left[1 - \exp(\frac{r^2}{2\sigma^2})\right] - d_{offset_y} \end{pmatrix} \tag{5.2.2}$$

where

$$\begin{gathered} r_x = x - x_{co} + x_{sep} \\ r_y = y - y_{co} + y_{sep} \\ r = x^2 + y^2 \end{gathered} \tag{5.2.3}$$

as already seen in the previous chapter.

Chapter 6

Particle tracking

In this chapter we will illustrate the principles and results of our tracking campaigns, aiming at studying the evolution of the charge distribution of the particles in the bunches which are closer to the beam pipe edges.

6.1 Optics parameters for the LHC

We define in the input files the properties of the machine, the crossing angle and the offset between the two beams at the IPs, the energy, the type of particles and the number of particles for each beam. In the optics file, we add markers in the points we are interested to, hence for these points the Twiss parameters and the one-turn-map are obtained from MAD-X.

We used the nominal LHC Optics, whose main parameters are summarised in the following table:

Nominal LHC	
Energy [TeV]	7
γ_{rel}	7460
n° of protons	$1.15\,10^{11}$
bunch distance [ns]	25
$\sigma_x[\mu m]$	1.6627
$\sigma_y[\mu m]$	1.6627
Q_x	62.31
Q_y	60.32
$\beta_x^*[m]$	0.55
$\beta_y^*[m]$	0.55
$\theta_c[\mu rad]$	300

Table 6.1.1: Optics parameters summary

6.2 Halo particles

There is no strict definition of when a particle belongs to the core or to the halo (or tail) of a distribution. An attempt [1] is to define an halo as a collection of particles of any origin and behavior which lies in the low density region of the beam distribution, far away from the core. "Far" refers to a distance equal to a certain number of times the rms transverse size of the beam.

We consider as halo particles those who are

- at the border of the dynamic aperture $n \cdot \sigma > 7\sigma$
- performing betatron oscillations with an amplitude commesurable with the collimators jaws aperture i.e. $r \gtrsim 5.7\sigma$[12]

Halo particles formation processes are a combination of different phenomena. By damping, these particles would normally lose betatron oscillation amplitude and leave slowly the halo to repopulate the beam core. Nevertheless, if there is an effect that keeps the halo population growing, such as the beam-beam effect, then instabilities and chaotic motion can be activated. In this case the halo would be responsible of beam losses i.e. particles absorption by physical elements of the machine. The collimators are elements that are spread throughout the accelerator ring to scrap the transverse dimensions of the beam in a controlled way in order not to have the energy of the loss beam deposited in the electronics or, especially, in the magnets. As the latter are superconducting and the energy of the lost particles directly transforms into heat, it is of primary importance to be able to absorb in a controlled way the losses.

Halo particles scraping directly affects the beam lifetime, i.e. the amount of time a good quality beam can be stored in the accelerator. If the halos are wide, then the collimators take out a big amount of charge from the beam at every pass. In Eq. (3.2.2) we saw that luminosity is directly proportional to the beam populations, so halo's expansion leads to luminosity reduction.

6.3 Particle distribution

Tracking 6D Gaussian distributions represents the bunch best, in particular with regards to chromatic effects, but for our purpose it is a rather inefficient distribution as most particles are located in the stable core, while the border of stability is only coarsely sampled. For a Gaussian, infact, the majority of the charged particles would be within 3σ radius from the center. Tracking a simple 3D Gaussian would not provide use with sufficient information about the particles at the border.

The approach we have used to achieve to our goal is

- to track a uniform distribution of particles in the (x,y) plane
- assign to each particle a certain percentage of charge density linked to the assigned initial conditions
- study the evolution of the current distribution of the halo particles

The weak strong approach allows for checks on the effect of the opposite beam on a non-Gaussian distribution to study the contributions of extended tails in addition to a Gaussian core. We may have significant non-gaussian tails which are hard to predict and simulate, but which may be quite important for machine protection and experimental conditions, as they cause machine induced background visible in the detectors.

Typically SixTrack simulates 60 particles at a time as they travel around the ring and runs the simulation for 10^5 loops (or sometimes 10^6). To be able to track a distribution of particles we have developed an automated procedure to launch parallel simulations of 60 particles, whose initial conditions would be taken from a fracion of the total uniform distribution. To run the tracking studies in parallel we have taken advantage of CERN server platform to launch batch of jobs remotely through a specific command. Using the run prolongation method we can custom defined entirely all the particles initial conditions by simply having SixTrack read them from the fort.13 file (see B).

6.3.1 Disk point picking method

To generate the initial uniform distribution, we first use a disk point picking algorithm on a unit radius circle area[7]. To generate random points over the unit disk, it is incorrect to use two uniformly distributed variables $r \in [0, 1]$ and $\theta \in [0, 2\pi)$ and then take

$$\begin{aligned} x &= r \cdot \cos\theta \\ y &= r \cdot \sin\theta \end{aligned} \tag{6.3.1}$$

Infact, the area element would then be

$$dA = 2\pi \cdot r \cdot dr \tag{6.3.2}$$

yielding a concentration of points dependent of the radius, thus densers in the center than in the outside.

The correct transformation is instead given by

$$\begin{aligned} x &= \sqrt{r} \cdot \cos\theta \\ y &= \sqrt{r} \cdot \sin\theta \end{aligned} \tag{6.3.3}$$

Now the probability function for distance d from the center of a point picked at random in a unit disk is

$$P(d) = 2d \tag{6.3.4}$$

yielding a mean distance value of $\bar{d} = 2/3$.

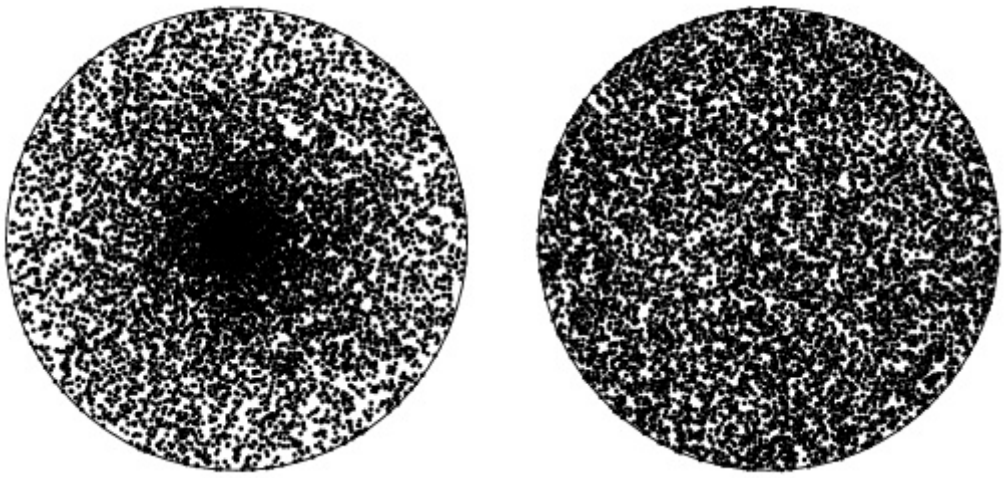

Figure 6.3.1: Left: points generated with equation (6.3.1); Right: correctly uniformly distributed points generated with equation (6.3.3)

To generate initial conditions of a bigger amplitude than the unit disk, we simply multiply the unit disk by the amplitude interval we want to track.

For what concerns the other parameters of the 6D phase space to initialise, we made two types of studies:

- with nominal energy and zero divergence in all planes
- with nominal energy and initial divergence $z' = [-\theta_c, \theta_c]$ *with* $z = x, y$ depending on the IP, as IP1 features a vertical crossing while IP5 features and horizontal one

By launching initial conditions of the first type though, we have found an error as the prolongation run utility in SixTrack requires the closed orbit to be added to the declared particles starting coordinates. So, it is necessary to launch particles with initial divergence matched to the one they would have at the interaction point.

Such initial coordinates are then automatically written, 60 by 60 and in the appropriate format, in a fort.13 file, that is stored together with the other needed SixTrack input files and the simulation is launched (see Appendix B).

6.3.2 Charge density distribution

The 2D charge density distribution is calculated from the initial conditions with the bidimensional normal distribution, which in the hypothesis of uncorrelated densities and round beams is equal to

$$G(x_0, y_0) = \frac{1}{2\pi\sigma^2} \exp\left(-\frac{(x_0 - \mu_x)^2}{2\sigma^2} - \frac{(y_0 - \mu_y)^2}{2\sigma^2}\right) \tag{6.3.5}$$

We used a Gaussian with standard deviation equal to the value of the rms transverse size of the beam i.e. $\sigma = \sigma_x = \sigma_y = \sqrt{\epsilon\beta*}$.

6.4 Particle tracking post-processing

At the end of each run, SixTrack returns the turn-by-N-turns 6D coordinates of each particle as binary files, where the value of N can be set by the user. As one can imagine such files can be quite big, so we have followed the recommendation of the SixTrack manual to use $N = 1000$, thus saving in memory 100 files per simulation. To analyse such files we have integrated a Python module[18] into a routine that reads the binary files and stores the coordinates values in a more accessible SQLite dB. From this dB then we have developed, once again in Python, tools to plot the data in several ways. In the following paragraphs we'll show the results of such post-processing routines and finally draw some conclusion from them.

The post-processing for each simulation consists of the following subplots:

- Top line:
  - transverse configuration space (x, y) in units of r.m.s. transverse beam size σ
  - horizontal configuration space (x, x') , respectively in units of r.m.s. beam size σ and divergence σ_p
- Bottom line:
  - vertical configuration space (y, y'), respectively in units of r.m.s. beam size σ and divergence σ_p
  - action space (J_x, J_y) in units of $[m \cdot rad]$

Of all the over 100 plots produced per each simulation, we will show only the most significant ones for each simulation.

Each simulation has been assigned a corresponds ID to clearly identify the dataset, whose parameters are summarised in the tracking studies overview table below. The IDs themselves contain a summary of the values, as they respect the format

$$IP\#\_numberofparticles\_amplitudeinsigmaunits\_x'_0initialy'_0\_numberofturns$$

Simulation ID	IP1_10E4_10_00.1475_10E4	IP5_10E4_10_0.14750_10E4
Number of particles	10 080	10 080
Disk radius	10σ	10σ
x'_0	0	[-0.1475,0.1475] mrad
y'_0	[-0.1475,0.1475] mrad	0
Interaction point	IP1	IP5
Number of turns	10^5	10^5
Beam-beam elements	17	17

Table 6.4.1: Summary of tracking parameters used per each simulation

6.4.1 Interaction Point 1 (ATLAS)

In this section we present the output of the post-processing of the simulation

IP1_10E4_10_00.1475_10E4

Figure (6.4.1) shows the initial conditions, as they are also recorded in the turn by turn data for $turn = 0$. This is useful both to provide the user a tool to check the program ran as expected, both as the starting point of the charge density distribution evolution. The colour contours of the plot indicate the charge density associated to each particle, according to the formula (6.3.5).

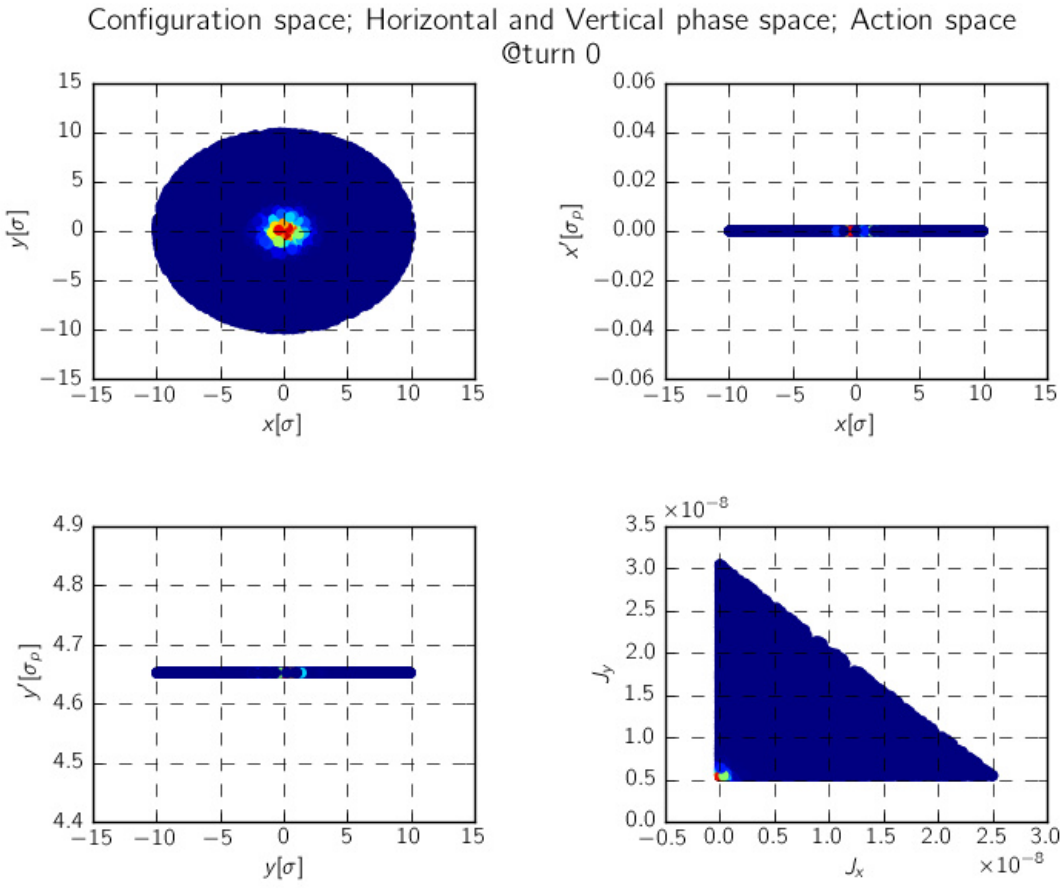

Figure 6.4.1: Initial configuration data at IP1. Top: transverse configuration space (x, y)(left), horizontal phase space(x, x')(right); bottom: vertical phase space(y, y')(left), action space(J_x, J_y)(right)

The next figure 6.4.2 shows the output of the post processing of the tracking data after 100 000 turns. By representing the quantities in units of single r.m.s. beam size and divergence, the plots clearly show how the more external particles deviate from the desidered trajectory and diffuse towards wider amplitude of betatron oscillation. Moreover, the action space plot highlights the presence of a non-linear process, as particles drift towards higher values.

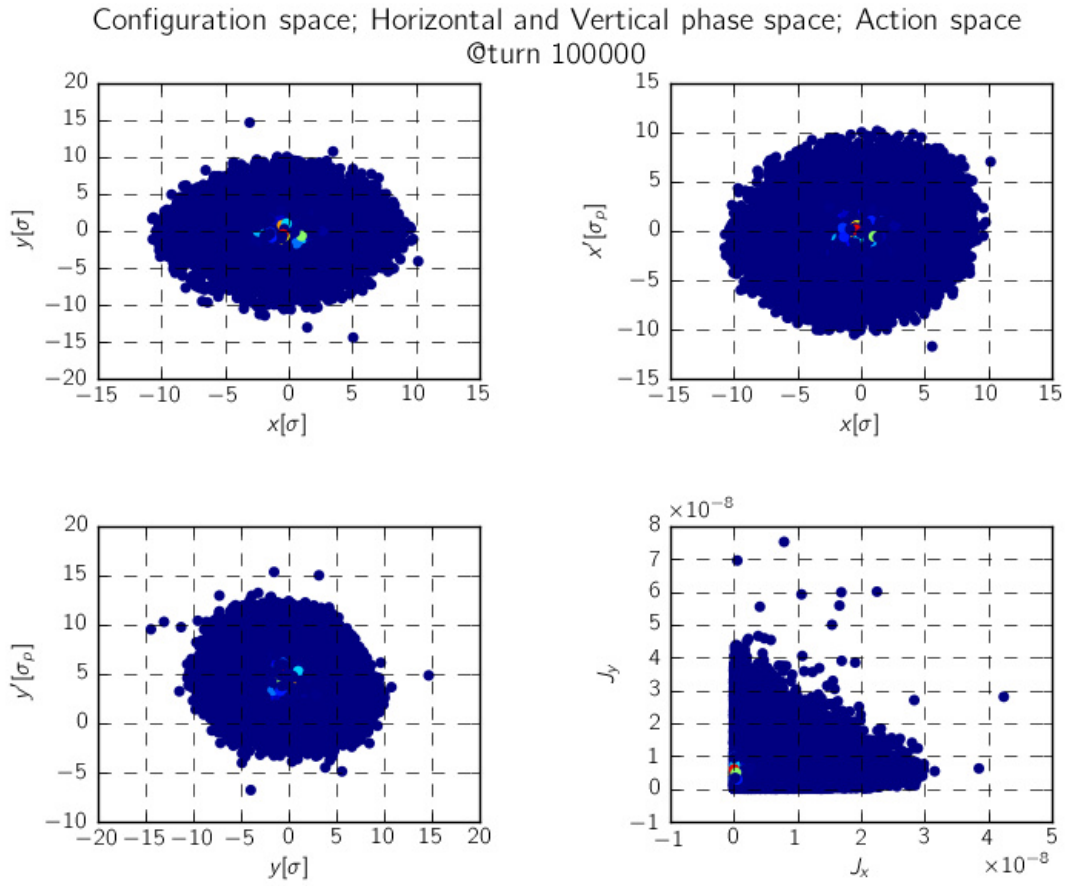

Figure 6.4.2: End-of-tracking data at IP1. Top: transverse configuration space (x, y)(left), horizontal phase space(x, x')(right); bottom: vertical phase space(y, y')(left), action space(J_x, J_y)(right).

In the IP1 there is a vertical crossing scheme, meaning the beams have a vertical angle $y'_{Xing} = 0.3mrad \cong 10\sigma'$ that would appear as an offset in the vertical phase space of figure (6.4.2). That's why in the post-processing this angle value is subtracted from the y' coordinates.

6.4.2 Interaction Point 5 (CMS)

In this section we present the output of the post-processing of the simulation

IP5_10E4_10_0.14750_10E4

Figure 6.4.3 shows the initial conditions, as they are also recorded in the turn by turn data for $turn = 0$. This is useful both to provide the user a tool to check the program ran as expected, both as the starting point of the charge density distribution evolution. The colour contours of the plot indicate the charge density associated to each particle, according to the formula (6.3.5).

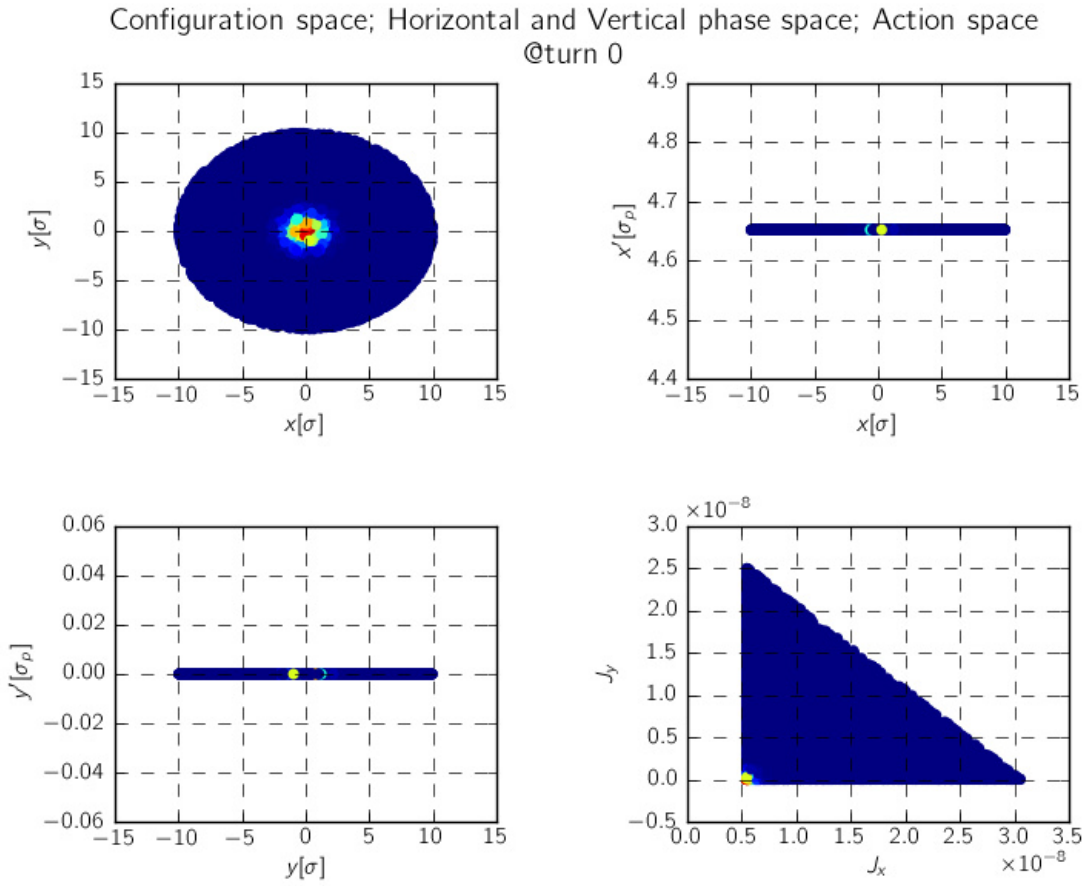

Figure 6.4.3: Initial configuration data at IP5. Top: transverse configuration space (x, y)(left), horizontal phase space(x, x')(right); bottom: vertical phase space(y, y')(left), action space(J_x, J_y)(right)

The next figure shows the output of the post processing of the tracking data after 100 000 turns. In comparison to the data of IP1, IP5 shows a less severe diffusion and halo particles appear closer to the beam core and suffer minor diffusion.

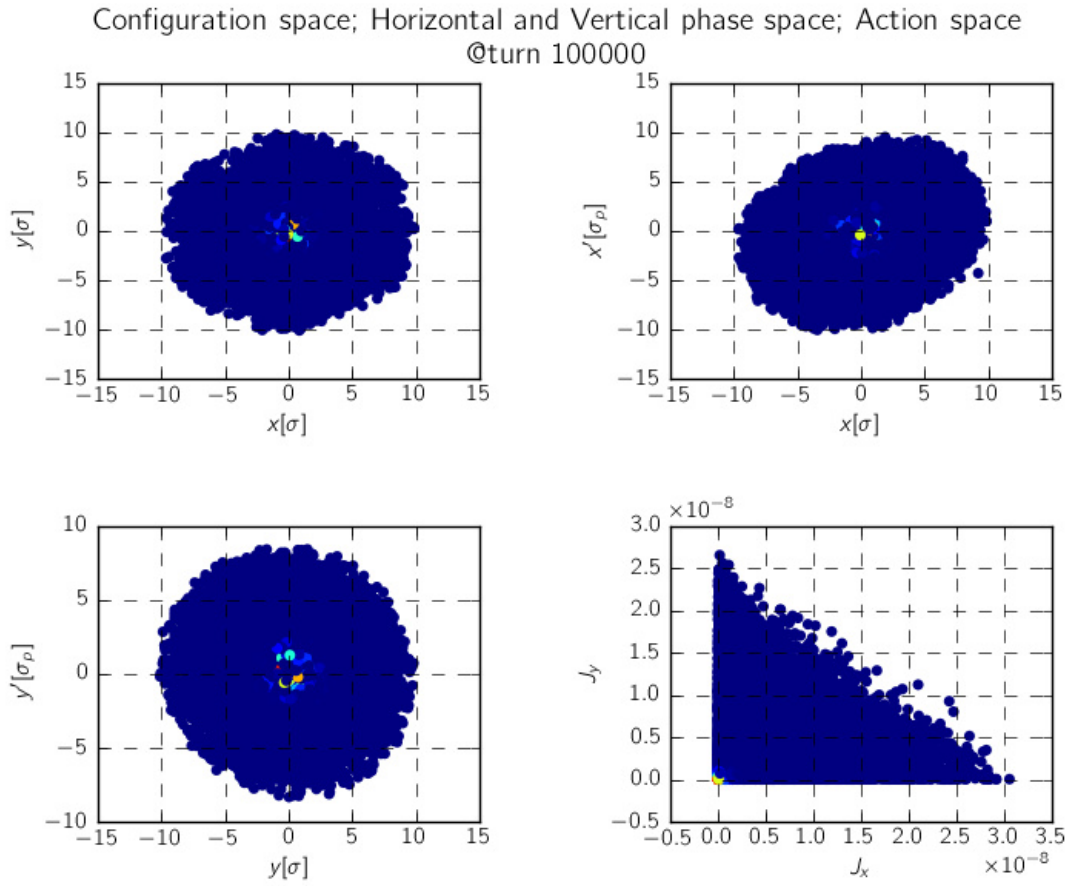

Figure 6.4.4: End-of-tracking data at IP5. Top: transverse configuration space (x, y)(left), horizontal phase space(x, x')(right); bottom: vertical phase space(y, y')(left), action space(J_x, J_y)(right).

In the IP5 there is a horizontal crossing scheme, meaning the beams have a horizontal angle $x'_{Xing} = 0.3mrad \cong 10\sigma'$ that would appear as an offset in the horizontal phase space of figure (6.4.4). That's why in the post-processing this angle value is subtracted from the x' coordinates.

6.4.3 Relative action variation

The action is defined as

$$J_z = \frac{z^2 + (\beta z')^2}{2} \text{ with } z = x, y \tag{6.4.1}$$

and in the absence of resonant phenomena is an invariant of motion. Thus, to analyse the presence of non-linear phenomena in the halos, we plot the relative action variation meaning

$$\Delta J = \frac{(J_x + J_y)_{turn=100000}}{(J_x + J_y)_{turn=0}} \tag{6.4.2}$$

For well-behaving particles, we would expect the ratio to be $\Delta J = 1$, while for resonant-behaving particles we would see a $\Delta J > 1$.

The following plots show the relative action variation versus initial amplitude in σ units.

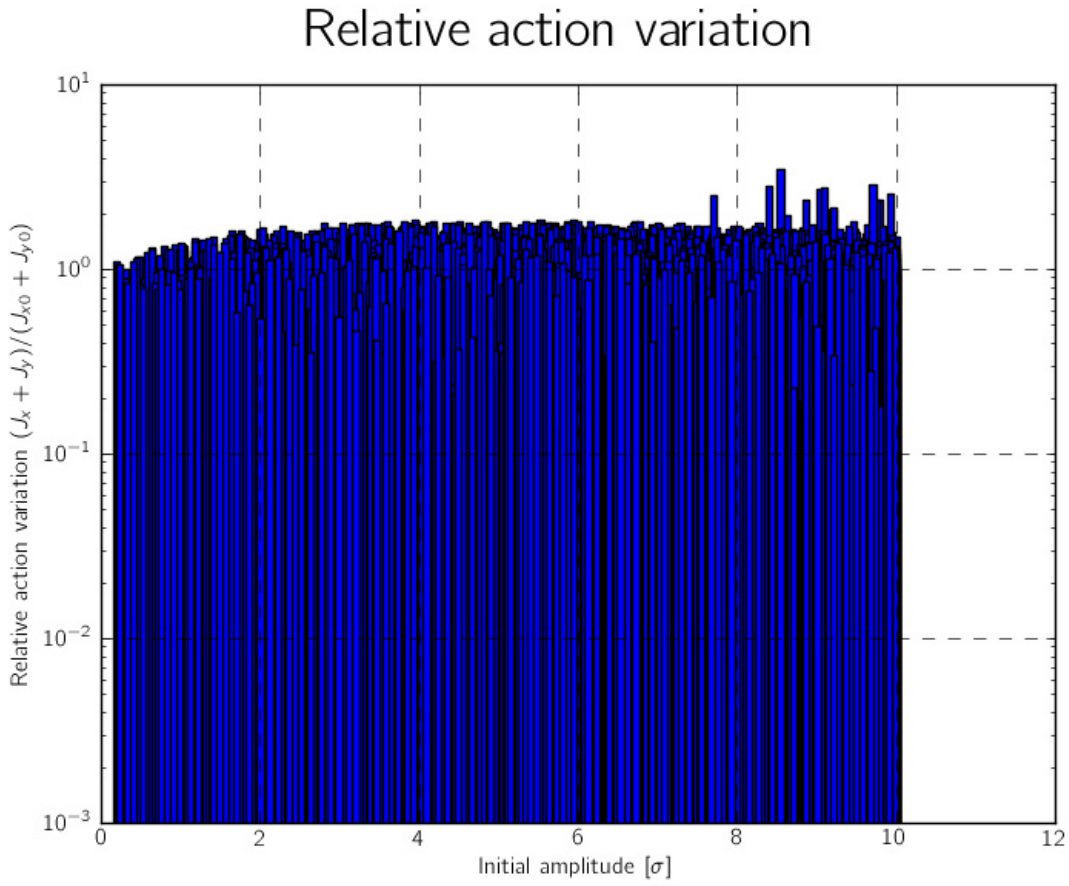

Figure 6.4.5: Relative action variation versus initial amplitude $r_0 = \sqrt{x_0^2 + y_0^2}$ in units of σ for IP1.

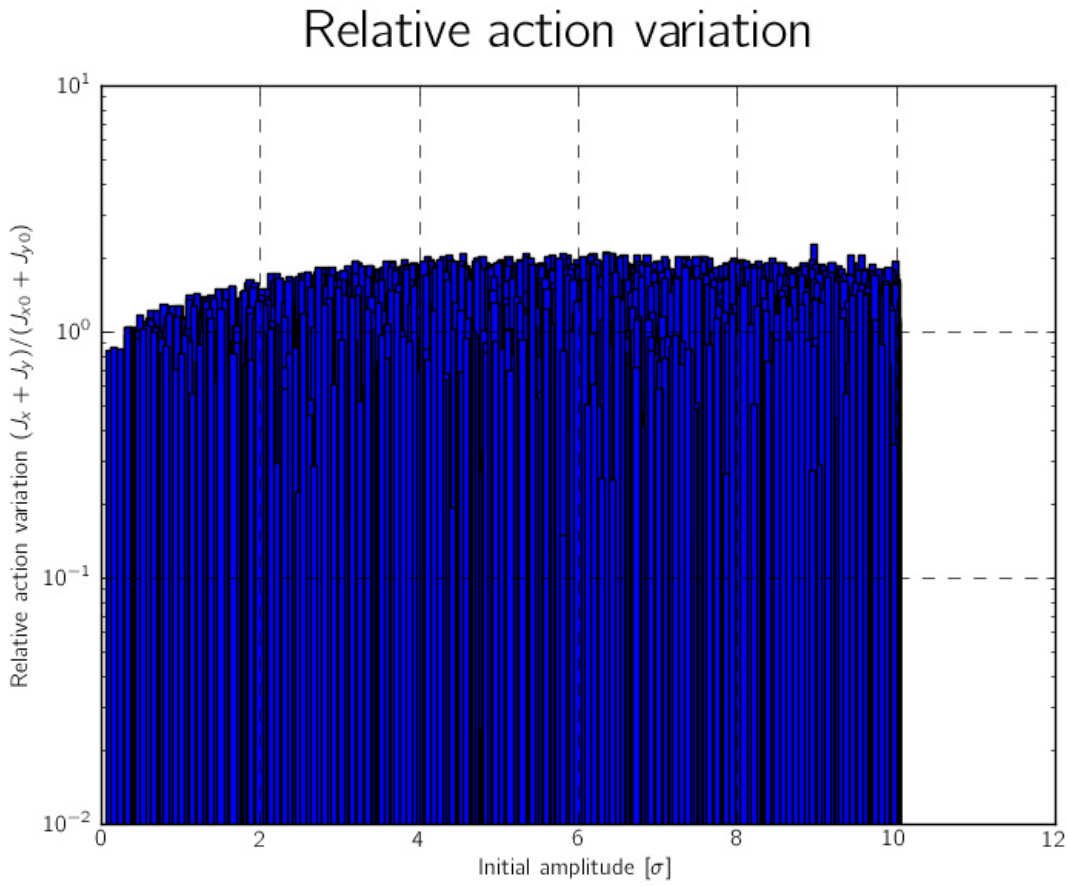

Figure 6.4.6: Relative action variation versus initial amplitude $r_0 = \sqrt{x_0^2 + y_0^2}$ in units of σ for IP5.

In both cases stability arises especially for particles with starting amplitude $r_0 > 7\sigma$, where the boundary between stable and chaotic region is expected to be. Moreover, we see again, and this time more vividly, that in IP1 the instabilities look more severe than in IP5.

6.4.4 Lost particles

At $r > 6.5\sigma$ beam losses start to appear. Figure 6.4.7 shows the number of lost particles per turn for IP1, while for IP5 no particles get lost.

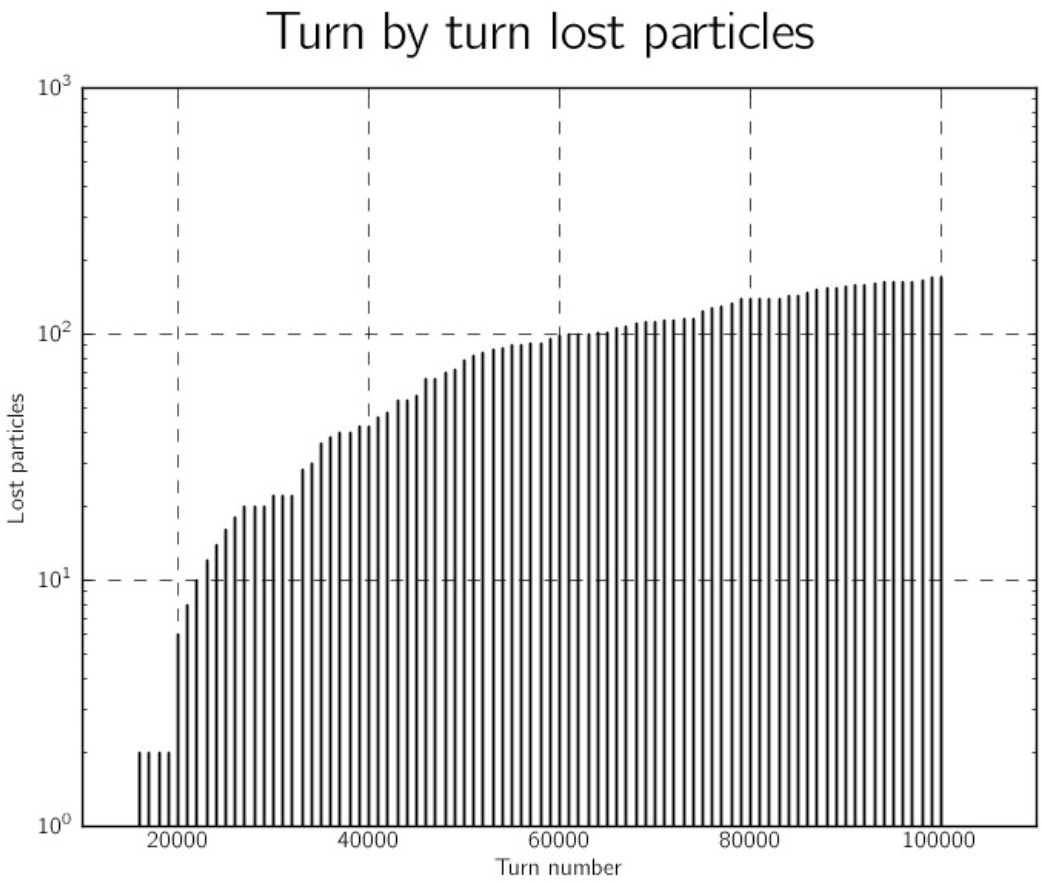

Figure 6.4.7: Lost particles at each turn for the simulation at IP1.

The data will be further analised to determine the best fitting growth rate for the phenomena.

We have also plotted the complementary data, meaning the number of particles survived at each turn, as illustrated in Figure 6.4.8 and 6.4.9.

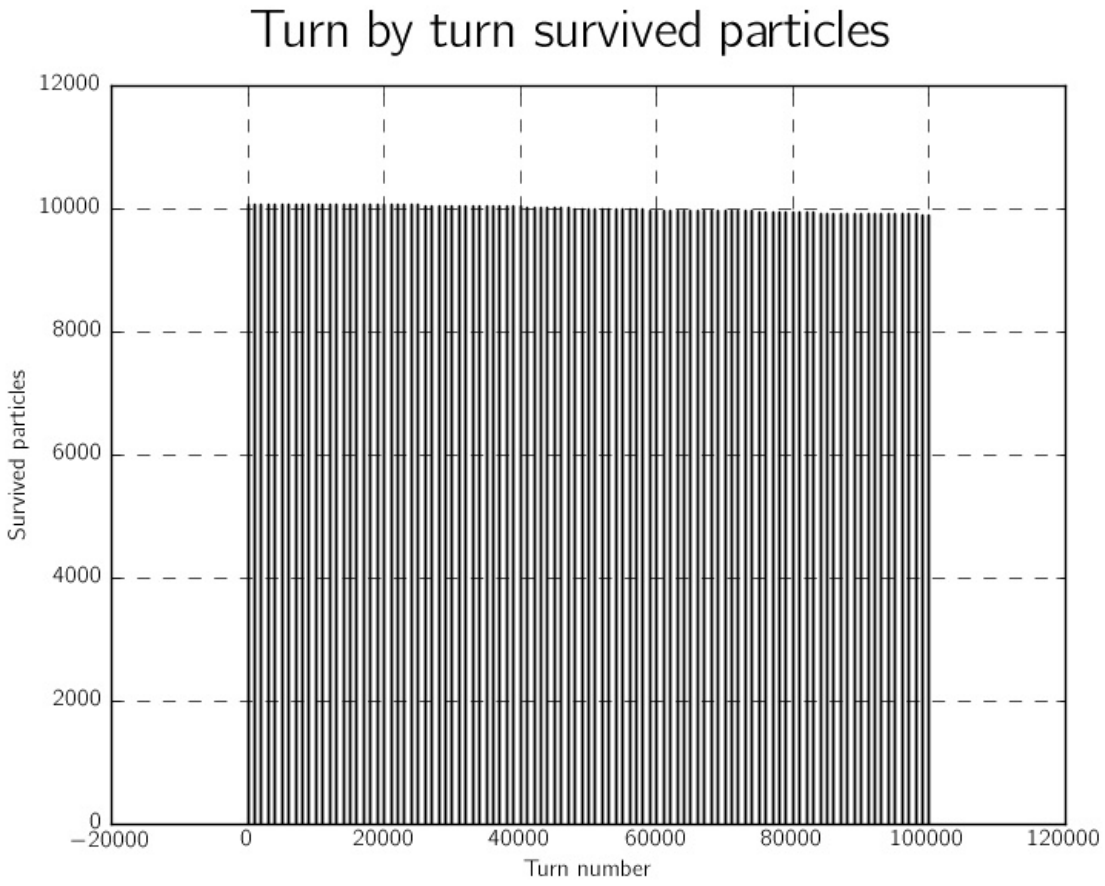

Figure 6.4.8: Survived particles at each turn for the simulation at IP1.

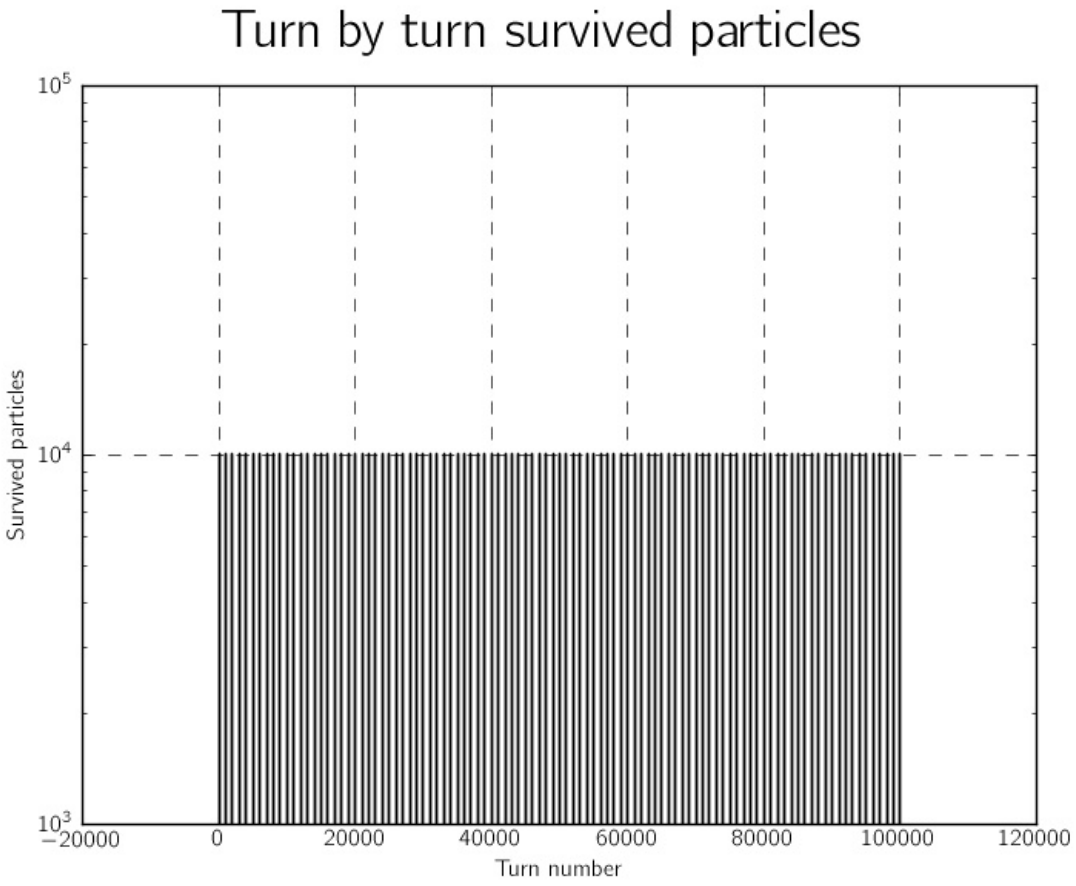

Figure 6.4.9: Survived particles at each turn for the simulation at IP5.

6.5 Conclusions

The data consistently shows that the beam-beam effect creates halo particles that diffuse towards the borders of dynamic and physical apertures. The effect looks to be more severe for the interaction region 1 and more contained for the symmetrical region 5. This could be an indication that the compensators along region 1 should be checked to reduce the detrimental effects of the beam-beam interaction.

Chapter 7

Summary

The Large Hadron Collider is the biggest and most energetic particle collider in the world. It is currently undergoing a long shutdown period of maintainance and upgrade, to advance our knowledge of the fundamental physical laws of the universe through the measurements of its experiment. Its key performance parameter, the luminosity, has not been completely modeled yet, especially concerning what are the high energy phenomena that could degrade it. The present work focused on the methodologies needed to enhance the model and it is the first milestone towards the development of a model of luminosity evolution, through the analysis of the causes of beam lifetime degradation.

We have illustrated the mathematical formalism used to study beam dynamics in any circular accelerator and presented the concept of symplecticity. Other key parameters presented to comprehend the beam dynamics that have been presented are: the thin lens approximation, the Courant-Snyder invariant and the emittance, the r.m.s. beam size and divergence, the tune. The definition of the latter has provided us with intuitive ways of understanding the circumstances that lead to a resonant behaviour of the betatron oscillations.

Next we have illustrated the state of the art of the luminosity models, exploiting in particular the parts of the model linked to the interaction between the beams at the interaction points. We've focused our attention on the description of this interaction, distinguishing between the head-on interaction and the long range one. Whe have illustrated the destabilizing potential of the phenomenon, and shown ways to limit it. Concerning the long-range beam-beam interaction, we have discussed it's impact on the beam dynamics in terms of transverse kick and characteristic detuning.

We have developed tools for conducting massive tracking studies on transversally uniformly distributed particles and for their post-processing analysis. The tracking has been done through SixTrack, a powerful open source symplectic integrator that has been developed within CERN and consolidated within the years. We have enhanced SixTrack power by developing pieces of code to add to it the possibility of tracking distribution of more than 60 particles per time, via parallel processing on the CERN servers. SixTrack is very well integrated with another software that we have been using, MAD-x, through which the accelerator optics were generated and the beam-beam kick matrices included in the model.

We have conducted studies on two interaction points called IP1 nad IP5, displaced at simmetrical locations along the ring, where the two biggest experiments, respectively

ATLAS and CMS, are situated.

We have launched tracking campaigns containing more than 10 000 particles over 100 000 revolution turns around the ring. Altough this translates to roughly 10 seconds of beam time in the LHC, it is sufficient to detect the emergence of desruptive behaviour.

We have plotted the transverse configuration space, phase space portraits, action space, relative action variation, turn by turn lost and survived particles. The data analysis has enabled us to study charge distribution evolution and to the detect instability of halo particles, especially around IP1.

Further developments of the work will include enhancing the number of particles and the extension of the halo, the development of more complex post-processing tools and integration of beam-beam correction schemes in the simulations. We want also to be able to later confront the simulation output with the experimental data collected in previous and in future runs.

Appendix A

Lagrangian of a charged particle in an electromagnetic field

Any function L that satisfyies Euler-Lagrange equations in n degrees of freedom

$$\sum_{j=0}^{n}\left[\frac{\partial L}{\partial q_j}-\frac{d}{dt}\frac{\partial L}{\partial \dot{q_j}}\right]=0 \tag{A.0.1}$$

can be the Lagrangian of a system. Thus, to determine which of all the possible Lagrangian is the right one to characterise a system is almost an artist work. In this appendix we will present one way to obtain the expression of the Lagrangian describing the motion of a charged particle in an electromagnetic field.

For a conservative force, the potential is independent of the derivative of the generalised coordinates, and thus the Lagrangian can be found as

$$L=T-U \tag{A.0.2}$$

where T represents the kinetic energy of the system and U the potential of the force acting on the system.

If the forces are not conservatives, to keep the same simple definition, one can define a generalised potential $U(q_j,\dot{q_j})$

$$U \quad | \quad Q=\sum_{j=0}^{n}\left[-\frac{\partial U}{\partial q_j}+\frac{d}{dt}\left(\frac{\partial U}{\partial \dot{q_j}}\right)\right] \tag{A.0.3}$$

where Q is called the *generalised force* and it is defined as

$$\sum \vec{F_j}\delta\vec{r_j}=\sum Q_j\delta q_j \tag{A.0.4}$$

The vectors $\vec{F}$ and $\vec{r}$ represent respectively the force and positition vectors in Cartesian coordinates. From this definition it follows that Q_j does not necessarily have the units of a force, but the product $Q\cdot\delta q$ is always in units of work, justifying the name.

Now let's focus on a system composed by a single charged particle under the action of an electromagnetic field. The active force on the system is the Lorentz force

$$\vec{F}=e(\vec{E}+\vec{v}\times\vec{B}) \tag{A.0.5}$$

Using the electromagnetic potentials, we can rewite the expession of the force as

$$\vec{F} = e\left(-\nabla\phi - \frac{\partial\vec{A}}{\partial t} + \vec{v}\times\nabla\times\vec{A}\right) \tag{A.0.6}$$

Let's analyse the horizontal component of such force in a Cartesian coordinates system:

$$F_x = e\left(-\nabla_x\phi - \frac{\partial A_x}{\partial t} + (\vec{v}\times\nabla\times\vec{A})_x\right) \tag{A.0.7}$$

We can expand the x-component of the vectorial product as

$$(\vec{v}\times\nabla\times\vec{A})_x = v_y\left(\frac{\partial A_y}{\partial x} - \frac{\partial A_x}{\partial y}\right) - v_z\left(\frac{\partial A_x}{\partial z} - \frac{\partial A_z}{\partial x}\right) \pm v_x\frac{\partial A_x}{\partial x} = \vec{v}\cdot\frac{\partial\vec{A}_x}{\partial x} - \left(\frac{dA_x}{dt} - \frac{\partial A_x}{\partial t}\right) \tag{A.0.8}$$

where we used the relation

$$\frac{dA_x}{dt} = \frac{\partial A_x}{\partial x}\frac{dx}{dt} + \frac{\partial A_x}{\partial y}\frac{dy}{dt} + \frac{\partial A_x}{\partial z}\frac{dz}{dt} + \frac{\partial A_x}{\partial t} \tag{A.0.9}$$

Now, plugging (A.0.8) in (A.0.7) we obtain a new expression of the force as

$$F_x = e\left[-\frac{\partial}{\partial x}\left(\phi - \vec{v}\cdot\vec{A}\right) - \frac{dA_x}{dt}\right] \tag{A.0.10}$$

Finally, we can observe that

$$\frac{dA_x}{dt} = \frac{d}{dt}\left[\frac{\partial}{\partial v_x}\left(\vec{v}\cdot\vec{A} - \phi\right)\right] \tag{A.0.11}$$

and thus rewite the component of the force as

$$F_x = e\left[-\frac{\partial}{\partial x}(\phi - \vec{v}\cdot\vec{A}) + \frac{d}{dt}\frac{\partial}{\partial v_x}\left(\phi - \vec{v}\cdot\vec{A}\right)\right] \tag{A.0.12}$$

If we now compare equation (A.0.12) with (A.0.3) we obtain the expression of the generalised potential as

$$U = e(\phi - \vec{v}\cdot\vec{A}) \tag{A.0.13}$$

and so we can write the Lagrangian as

$$L = T - U = T - e(\phi - \vec{v}\cdot\vec{A}) \tag{A.0.14}$$

For a relativistic particle, the kinetic energy is

$$T = \int\vec{p}\cdot\delta\vec{v} = -mc^2\sqrt{1 - \frac{v^2}{c^2}} \tag{A.0.15}$$

and thus we obtain the final expression of the Lagrangian to be

$$L = -\frac{mc^2}{\gamma} - e(\phi - \vec{v}\cdot\vec{A}) \tag{A.0.16}$$

Appendix B

SixTrack input files

The input data needed to run SixTrack are:

- the description of an accelerator,
- the definition of the starting point of the tracking and
- the initial 6D coordinates of the particles one wants to track.

All of this is fully contained in four input files. We will briefly present their function and how they are produced. All SixTrack files are named fort.n, where n is an integer. For brevity we will omit the fort. part of the name and replace it with a hashtag character.

- #2 unit: the geometry file, and contains the accelerator lattice optics
- #3 unit: the parameters file, in which all the relevant parameters for a simulation are defined by the user
- #8 unit: random numbers of the single multipole kick, the horizontal and vertical misalignment and the value of the tilt
- #16 unit: multipole errors

To write the geometry file by hand would be rather inconvenient. The optics definition is thus done within the framework of MAD. The SIXTRACK optics files are transferred from MAD-X, that generates them through a ".mask" input file.

B.1 Simulation parameters

SixTrack input file for simulation parameters is the unit #3, where there are several blocks and options that can be customly defined by the user for its specific purposes. We'll briefly go through the most significant of such blocks and parameters, which are the Tracking and Initial coordinates ones**(author?)** [8].

For the study of nonlinear system the choice of initial conditions is of crucial importance. The input structure for the initial conditions was therefore organise in such a way as to allow for maximum flexibility. SixTrack is optimised to reach the largest possible number of turns. In order to derive the Lyapunov exponent and thereby to distinguish between regular and chaotic motion, the particle has a close by companion particle.

```
TRACKING BLOCK ------------------------
numl numlr napx amp(1) amp0 ird imc data
idy(1) idy(2) idfor irew iclo6
nde(1) nde(2) nwr(1) nwr(2) nwr(3) nwr(4) ntwin ibidu iexact
```

```
INITIAL COORDINATES BLOCK -------------
itra chi0 chid rat iver
data lines 2 to 16: 15 initial coordinates
```

B.1.1 Tracking parameters block

All tracking parameters are defined with this input block, the initial coordinates are generally set here, too. This block is identified by the keyword TRACK, that can be then followed by other random characters. It generally looks like this:

where the names represent numbers which are set by the user, and they mean different things depending to which variable they are assigned. In particular:

- numl (integer) : number of turns in the forward direction
- napx (integer): number of amplitude variations
- amp(1), amp0 (floats): start and end amplitude (any sign) in the horizontal phase space plane for the amplitude variations of the betatron and oscillations
- idfor: Usually the closed orbit is added to the initial coordinates. This can be turned off using idfor, for instance when a run is to be prolonged.
    - if idfor = 2 then the initial coordinates are taken from unit # 13 instead then from the TRAC and/or INIT blocks

B.1.2 Initial conditions block

The Initial Coordinates input block is meant to manipulate how the initial coordinates are organised, which are generally set in the tracking parameter block. Number of particles, initial phase, ratio of the horizontal and vertical emittances and increments of 2×6 coordinates of the two particles, the reference energy and the starting energy for the two particles. This block is identified by the keyword INIT, that can be then followed by other random characters. It generally looks like this:

data line	contents
2	x_1 [mm] coordinate of particle 1
3	x'_1 [mrad] coordinate of particle 1
4	y_1 [mm] coordinate of particle 1
5	y'_1 [mrad] coordinate of particle 1
6	path length difference 1 ($\sigma_1 = s - v_o \times t$) [mm] of particle 1
7	$\frac{\Delta p}{p_{o1}}$ of particle 1
8	x_2 [mm] coordinate of particle 2
9	x'_2 [mrad] coordinate of particle 2
10	y_2 [mm] coordinate of particle 2
11	y'_2 [mrad] coordinate of particle 2
12	path length difference ($\sigma_2 = s - v_o \times t$) [mm] of particle 2
13	$\frac{\Delta p}{p_{o2}}$ of particle 2
14	energy [MeV] of the reference particle
15	energy [MeV] of particle 1
16	energy [MeV] of particle 2

Figure B.1.1: Initial coordinates set-up

These 15 coordinates are taken as the initial coordinates if itra is set to zero. If itra = 1 or 2, these coordinates are added to the initial coordinates generally defined in the tracking parameter block. This procedure seems complicated but it allows freely to define the initial difference between the two twin particles. It also allows in case a tracking run should be prolonged to continue with precisely the same coordinates. This is important as small difference may lead to largely different results.

B.1.3 Run prolongation method

A feature is installed for a prolongation of a run by using idfor = 2 and reading the initial data from unit #13. As our goal is to track a user defined distribution, we are using this feature to feed the program with the initial coordinates the user wants. The only limit to this is that only 60 particles per time can be tracked, so if one has a bigger distribution, as in our case, it must be sliced in groups of 60 particles. The unit #13 file is made of 1 column containing 30 repetitions of the data structure in Fig. B.1.1, for each group of two particles the user wants.

Ringraziamenti

Un sincero ringraziamento va innanzitutto nuovamente al Prof. Luigi Palumbo, per avermi dato l'opportunità di lavorare a questa tesi e per l'opera generosa di guida nel mondo della ricerca.

Ringrazio il Dott. Papaphilippou per avermi accolto tra i suoi collaboratori con la massima disponibilità e per avermi fatto crescere sul piano scientifico. Tra i colleghi del CERN vorrei poi ringraziare in particolare il Dott. Riccardo De Maria e la Dott.ssa Andrea Santamaria Garcia per la fruttuosa collaborazione istaurata in questi mesi. Ancora, un ringraziamento sincero al Prof. Andrea Mostacci, per la presenza costante negli anni come punto di riferimento per dubbi e consigli.

Ad ingegneria si inizia il percorso in tanti ma si finisce in pochi. Tra quei pochi colleghi con cui ho condiviso tutto il percorso accademico, vorrei ringraziare soprattutto il Dott. Francesco Massimo, per il costante confronto ed incoraggiamento che mi ha aiutato ad affrontare le sfide accademiche e lavorative.

Bibliography

[1] A. Fedotov, *Halo formation in High-Intensity Beams.* BNL Collider-Acceleration Department, 2005.

[2] A. Latina, *Transvers Dynamics.* JUAS Lecture, Archamps (2014). https://indico.cern.ch/event/286275/contribution/47/material/slides/0.pdf

[3] B. Holzer, *Transverse Dynamics I.* CAS lecture, Frascati (2008). *http://cas.web.cern.ch/cas/Italy%202008/Lectures/PDFs/Holzer-1.pdf*

[4] *CERN faq - LHC the guide, CERN-Brochure-2009-003-Eng.*

[5] Collisions group, http://lhc-machine-outreach.web.cern.ch/lhc-machine-outreach/collisions.htm (2014)

[6] D.A. Edwards and M.J.Syphers, *An introduction to the physics of high energy accelerators.* New York, NY : Wiley, 1993 (Repr. 2004)

[7] E.W. Weisstein, *Disk Point Picking.* From MathWorld–A Wolfram Web Resource. http://mathworld.wolfram.com/DiskPointPicking.html

[8] F. Schmidt, *SixTrack User's Reference Manual.*

[9] H. Goldstein, C. P. Poole Jr., J. L. Safko, *Classical Mechanics. 3rd ed. San Francisco, CA : Addison-Wesley, 2002.*

[10] J. Rossbach, P. Schmüser, *Basic course on accelerator optics.* Proceedings of the. 1992 CERN Accelerator School, CERN 94-01, (1994), p.17-88.

[11] K. Wille, *The physics of particle accelerators: an introduction. Oxford : Oxford Univ. Press, 2000 (Repr. 2005).*

[12] LHC Collimation project. http://lhc-collimation-project.web.cern.ch (2014)

[13] LHC@HOME project, http://lhcathome.web.cern.ch/ (2014)

[14] L. Palumbo, *Lezioni del corso di Fisica Moderna - Dall'elettrodinamica relativistica agli acceleratori di particelle.* Rev. 04, A.A. 2008/2009.

[15] M. Reiser, *Theory and design of charged particle beams. 2nd ed. Weinheim : Wiley, 2008.*

[16] M. Schaumann, *Beam-Beam Interaction Studies at LHC* - CERN, 2011.

[17] R. De Maria, M. Fjellstrom, *SixTrack Physics Manual.*

[18] SixDesk GitHub repository. https://github.com/SixTrack/SixDesk

[19] S.Y. Lee, *Accelerator Physics. 3rd ed. Singapore : World Scientific, 2012.*

[20] S. Kheifets, PETRA-Kurzmitteilung 119 (DESY 1976).

[21] T. Rijoff, *Testing long range beam-beam compensation for the LHC luminosity upgrade.* CERN, 2012.

[22] U. Dorda, *Compensation of long-range beam-beam interaction at the CERN LHC.* PhD thesis, CERN, 2008.

[23] W. Herr, *Concept of luminosity.* CAS Lecture, Daresbury (2007). https://cas.web.cern.ch/cas/UK-2007/Lectures/PDF/Herr/Herr-luminosity.pdf

[24] W. Herr and B. Muratori. *Concept of luminosity*, Zeuthen, Germany, pp. 361-378, (2003).

[25] W. Herr. *Beam-Beam Effects*, Cockcroft Institute Lectures (2009). http://zwe.home.cern.ch/zwe/talks/cockcroftbeambeam.pdf

[26] W. Herr, *A MAD-X Primer.* http://cds.cern.ch/record/744163/files/p505.pdf (2014)

[27] W. Herr, *Effects of the PACMAN bunches in the LHC.* LHC-Project-Report-39.

[28] Y. Papaphilippou, *Imperfections.* JUAS lecture, Archamps (2013). http://yannis.web.cern.ch/yannis/teaching/nonlinear_2013.pdf

[29] Y. Papaphilippou, *Non-linear dynamics.* Cockroft Institute Academic Training Program, Daresbury, UK, October 9-11, 2013.

[30] Y. Papaphilippou, F. Zimmermann, Weak-strong beam-beam simulations for the Large Hadron Collider. Phys. Rev. ST Accel. Beams 2, 104001 (1999).